Satellite Attitude Control

Using Magnetorquers
with Magnetic Dipole Moment Cancellation

Master Thesis

Rasmus Holst
Aalborg University, 2014

Institute of Electronic Systems
Control Engineering
Fredrik Bajers vej 7
9220 Aalborg Øst
Phone 99 40 86 00
http://es.aau.dk

Title:
Satellite Attitude Control Using Magnetorquers With Magnetic Dipole Moment Cancellation

Theme:
Master's thesis

Projectperiod:
April 2014 to August 2014

Projectgroup:
1035

Participants:
Rasmus Holst

Supervisor:
Jesper Abildgaard Larsen

Number of printed copies: 3

Number of pages: 87

Appendices: 3

Finished on: August 15, 2014

Synopsis:

This thesis describes the design and analysis of a nonlinear attitude control system for a CubeSat sized satellite based on the structure of the AAUSAT satellites.
An analysis of the main disturbances is made with the conclusion that only the magnetic dipole moment needs to be taken into account when performing attitude control, as this disturbance is 10 times larger than the rest combined.
An estimation of the satellite dipole moment is made as a bias estimation by an Extended Kalman Filter. The resulting estimate is correct within 8 % of the true dipole moment when estimating on data basen on a slowly tumbling satellite with state noise.
A sliding mode controller is used as the nonlinear controller and uses the magnetic dipole estimate from the Extended Kalman Filter to counteract this disturbance. The result is a controller capable of following a Nadir reference within an axis-wise error of 10 degrees. The downside to the controller is the constant power consumption needed, in order to counteract the magnetic dipole moment of the satellite.

Preface

This thesis covers the development of a attitude control system designed for implementation on a CubeSat sized satellite. The work is made as a Master's thesis at the Department of Electronic Systems at Aalborg University in the period April 2014 to August 2014.

The calculations for the presented work are made in Matlab with the simulations implemented in Simulink. The base structure of the Simulink model is developed by previous project groups working on the AAUSAT project and modified to work with the developed controller and disturbances. The implemented parameters and simulation structure are presented in appendix A.

A thank you should be given by the author to Associate Professor Jesper A. Larsen for supervising the project throughout the project period. Further thanks should be given to the students who have previously been working on the AAUSAT projects for the work of determining satellite parameters and development of simulation tools.

Rasmus Holst

Contents

List of Figures

Nomenclature

${}^{b}_{a}\mathbf{A}$	Rotation matrix from a to b
$\mathbf{B}$	Magnetic field from Earth
$\mathbf{E}$	Identity matrix
$\mathbf{I}$	Inertia matrix
$\mathbf{m}$	Dipole moment
$\boldsymbol{\Omega}$	Vector containing angular velocities
ω_o	Orbit rate
${}^{b}_{a}\mathbf{q}$	Attitude quaternion
$\bar{\mathbf{q}}$	Imaginary part of a quaternion
q_4	Real part of a quaternion
$\mathbf{S}[\cdot]$	Skew symmetric representation
${}^{i}\mathbf{v}$	Vector in i-frame
$\dot{\mathbf{q}}$, $\dot{\boldsymbol{\Omega}}$	Time derivative of $\mathbf{q}$, $\boldsymbol{\Omega}$
V	Lyapunov Candidate Function

Part I

Introduction

1 Introduction

About the thesis

This thesis covers the devopment of a attitude control system designed for implementation on a CubeSat sized satellite. The satellite used in this project is a CubeSat satellite build at Aalborg University in the section of Automation and Control. Furthermore the thesis also covers the estimation of the satellite's magnetic dipole moment, and will be used in the control structure to counteract the disturbance caused by this magnetic dipole.

1.1 AAUSAT

The AAUSAT-project is currently counting three launched satellites and further two is scheduled for launch shortly. All five satellites are designed as single unit sized CubeSats, all actuated by magnetorquers and operating in Low Earth Orbit (LEO).

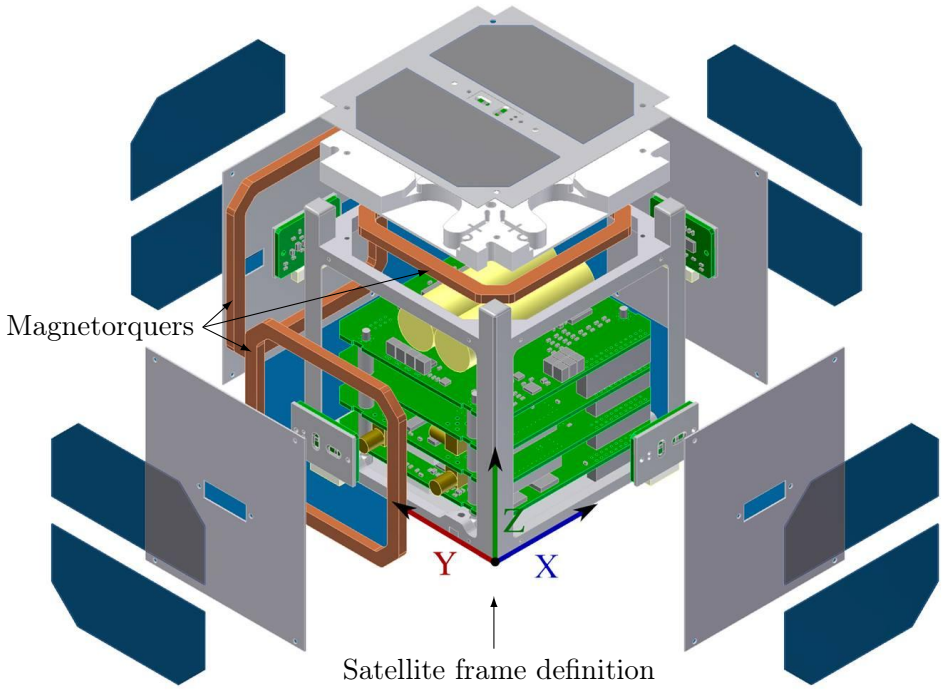

Figure 1.1: Exploded view of the AAUSAT satellite

From figure 1.1 an exploded view of the AAUSAT3 and AAUSAT4 is shown. The exploded view of the satellite shows three magnetorquers placed mutually perpendicular to each other, aligning these perpendicular to the x-, y- or z-axis of the satellite body respectively.

Mission specifications

Throughout the report, mission specific parameters are needed to determine the satellite behavior wrt. the environment. The parameters used in this report is based on the AAUSAT-3 structure and orbit, and, unless otherWise mentioned, are as listed in appendix A.

1.2 Coordinate Systems

In order to describe the environment of the satellite, several different coordinate systems are used. Some coordinate systems origins at the Earth while others use the satellite itself. In the subsequent paragraphs the different coordinate systems used in this text is described. It should be noted, that every mentioned coordinate system are right hand orthogonal systems.

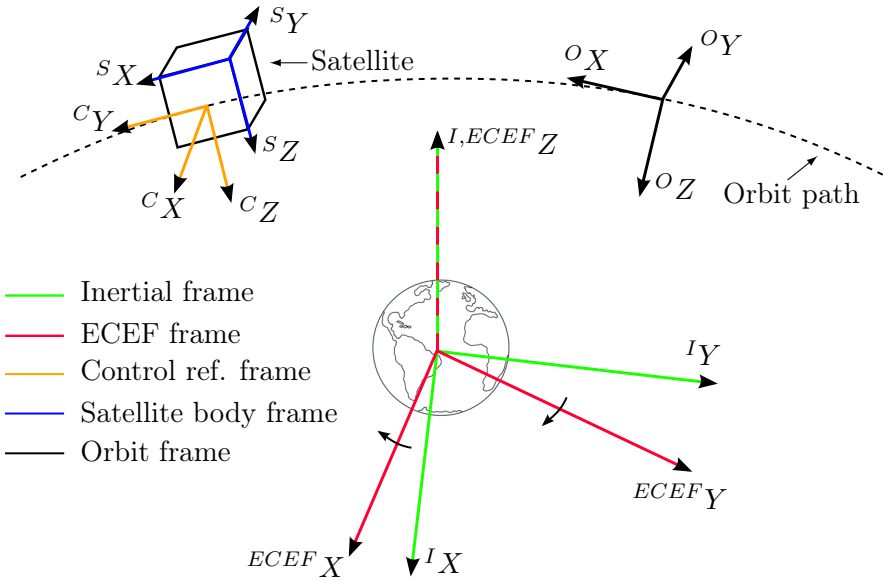

Figure 1.2: The used coordinate systems shown relative to each other. The illustration is not scalable.

Orbit CS

The Orbit coordinate system origins at the Satellites centre of mass with the z-axis pointing from the satellite towards the Earths centre of mass. The y-axis

points in the direction of the orbit velocity vector while the x-axis completes the system.
Frame superscript: O

Inertial CS

The Inertial coordinate system has its origin at the Earths centre of mass. The z-axis is parallel to the Earths axis of rotation and points towards the North Pole. The x-axis spans from the centre of Earth to Vernal Equinox[1]. The y-axis completes the coordinate system.
Frame superscript: I

ECEF CS

The Earth-centered Earth-fixed coordinate system has the origin at the Earths centre of mass and shares the z-axis with the Inertial CS. The x- and y-axis aligns with the corresponding axes in the Inertial CS on the initial Julian date. After this, it follows Earth's rotation.
Frame superscript: $ECEF$

Satellite body CS

The Satellite body coordinate system is fixed in the satellite. The coordinate system originates at a corner of the physical satellite frame as defined on figure 1.1. The z-axis is defined to be perpendicular to the antenna side of the body. The sensor measurements will be made in this frame.
Frame superscript: S

Control reference CS

The Control coordinate system is used to simplify the inertia matrix later on. This coordinate system has the origin in the satellite centre of mass with its principal axes fixed relative to the axes of the Satellite body CS. The x-axis is the axis with maximal moment of inertia and the z-axis is the one with the lowest moment of inertia.
Frame superscript: C

1.3 Rotations

The project contains multiple coordinate systems, and rotations of measurements and attitude representations between the coordinate systems are needed. Methods of this is described below using rotation matrices and quaternions.

[1] Vernal Equinox is the point where the ecliptic crosses the equator on the first day of spring.

Rotation matrices

The orientation of a vector (e.g. a measurement or heading) in a given coordinate system can be expressed in another coordinate system by the use of a rotation matrix.

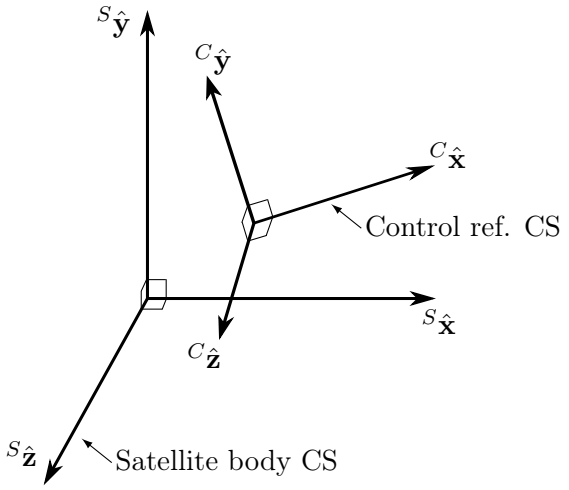

Figure 1.3: Coordinate system within a reference coordinate system.

The rotation between two coordinate systems, for instance from the Satellite body frame to the Control ref. frame, as seen on figure 1.3, can be described by the rotation matrix [[Wertz, 1994]]

$$ {}^{C}_{S}\mathbf{A} = \begin{bmatrix} {}^{C}x_{[^{S}x]} & {}^{C}x_{[^{S}y]} & {}^{C}x_{[^{S}z]} \\ {}^{C}y_{[^{S}x]} & {}^{C}y_{[^{S}y]} & {}^{C}y_{[^{S}z]} \\ {}^{C}z_{[^{S}x]} & {}^{C}s_{[^{S}y]} & {}^{C}z_{[^{S}z]} \end{bmatrix} \tag{1.1} $$

where ${}^{C}is_{j}$ is the representation of ${}^{S}j$ onto the ${}^{C}i$ axis.

A vector given in the Satellite body frame can by this approach be described in the Control ref. frame by using the rotation matrix as

$$ {}^{C}\mathbf{v} = {}^{C}_{S}\mathbf{A}\,{}^{S}\mathbf{v} \tag{1.2} $$

The rotation matrix will in this report mostly be used to perform measurement operations. This could for instance be gyroscope- or magnetometer measurements in the Satellite body frame that needs to be transformed into coordinates of the Control ref. frame.

The rotation matrix can also be used to perform operations on the attitude representation of the satellite, but it has a serious disadvantage; the Euler angles can represent the same orientation in multiple ways, leading to singularities. This can be avoided by using quaternions as described in the next section.

Quaternions

The quaternions provide a singularity-free describtion of the orientation with only four parameters. The quaternion consists of three imaginary parts and a single real part and can be expressed as [[Wertz, 1994]]

$$\mathbf{q} = \mathbf{i}q_1 + \mathbf{j}q_2 + \mathbf{k}q_3 + q_4 \tag{1.3}$$

or with the imaginary part contracted as

$$\mathbf{q} = \bar{\mathbf{q}} + q_4 \tag{1.4}$$

A unit quaternion can be rotated about the vector $\mathbf{n} = [n_1 \quad n_2 \quad n_3]^\intercal$ at an angle ϕ, by the equations:

$$\begin{aligned} q_1 &= n_1 \sin\frac{\phi}{2} \\ q_2 &= n_2 \sin\frac{\phi}{2} \\ q_3 &= n_3 \sin\frac{\phi}{2} \\ q_4 &= \cos\frac{\phi}{2} \end{aligned} \tag{1.5}$$

The unit quaternion satisfies the constraint

$$\mathbf{q}^\intercal\mathbf{q} = \bar{\mathbf{q}}^\intercal\bar{\mathbf{q}} + q_4^2 = q_1^2 + q_2^2 + q_3^2 + q_4^2 = 1 \tag{1.6}$$

By this constraint it is seen that the quaternion representation of the rotation between two aligning frames is

$${}^b_a\mathbf{q} = [q_1 \quad q_2 \quad q_3 \quad q_4]^\intercal = [0 \quad 0 \quad 0 \quad 1]^\intercal \tag{1.7}$$

The quaternion rotation between coordinate systems are used extensively throughout the report. The quaternion representing the rotation from the Satellite body frame to the Control reference frame can be written as

$${}^C_S\mathbf{q}. \tag{1.8}$$

A convenient feature of representing attitude by quaternions is the method for calculating succesive rotations. A rotation can for instance be calculated as

$${}^2_1\mathbf{q} = {}^3_1\mathbf{q} \otimes {}^2_3\mathbf{q} \tag{1.9}$$

or equivalently by

$${}^2_1\mathbf{q} = \mathbf{S}\left({}^2_3\mathbf{q}\right)\ {}^3_1\mathbf{q} \tag{1.10}$$

with $\mathbf{S}(\mathbf{q})$ being the skew-symmetric matrix

$$\mathbf{S}(\mathbf{q}) = \begin{bmatrix} q_4 & q_3 & -q_2 & q_1 \\ -q_3 & q_4 & q_1 & q_2 \\ q_2 & -q_1 & q_4 & q_3 \\ -q_1 & -q_2 & -q_3 & q_4 \end{bmatrix} \tag{1.11}$$

The quaternion can be used for vector rotation as well. To do this, the imaginary part of the quaternion is used. This gives:

$${}^{C}\mathbf{v} = {}^{C}_{S}\mathbf{q}^{*} \otimes {}^{S}\mathbf{v} \otimes {}^{C}_{S}\mathbf{q} \tag{1.12}$$

with ${}^{C}_{S}\mathbf{q}^{*}$ being the conjugate of ${}^{C}_{S}\mathbf{q}$ and ${}^{S}\mathbf{v}$ is the 3-dimensional vector augmented like $[v_x \quad v_y \quad v_z \quad 0]^{\intercal}$.

The rotation matrix from eq. (1.1) can be represented by quaternions as

$${}^{C}_{S}\mathbf{A} = \begin{bmatrix} {}^{C}\mathbf{i}_S & {}^{C}\mathbf{j}_S & {}^{C}\mathbf{k}_S \end{bmatrix} \tag{1.13}$$

where e.g. $\mathbf{k}_S$ is the z-axis of the Satellite body frame given in the Control reference frame. By parameterizing by quaternions the vectors become:

$${}^{C}\mathbf{i}_S = \begin{bmatrix} q_1^2 - q_2^2 - q_3^2 + q_4^2 & 2(q_1q_2 - q_3q_4) & 2(q_1q_3 + q_2q_4) \end{bmatrix}^{\intercal} \tag{1.14}$$

$${}^{C}\mathbf{j}_S = \begin{bmatrix} 2(q_1q_2 + q_3q_4) & -q_1^2 + q_2^2 - q_3^2 + q_4^2 & 2(q_2q_3 - q_1q_4) \end{bmatrix}^{\intercal} \tag{1.15}$$

$${}^{C}\mathbf{k}_S = \begin{bmatrix} 2(q_1q_3 - q_2q_4) & 2(q_2q_3 + q_1q_4) & -q_1^2 - q_2^2 + q_3^2 + q_4^2 \end{bmatrix}^{\intercal} \tag{1.16}$$

This could for instance be used to calculate the angular velocity relation between multiple frames

$${}^{S}_{O}\mathbf{\Omega} = {}^{S}_{I}\mathbf{\Omega} - \omega_O {}^{S}\mathbf{j}_O \tag{1.17}$$

Part II

Modeling

Kinematic and Dynamic Model

2

This chapter describes the modeling of the kinematics and dynamics of a rigid spacecraft. The equations contains inputs from actuators and disturbances, these will be presented in the next chapter.

2.1 Kinematic

The kinematic equation presented here is the motion of a rigid spacecraft, described as the rotation from an orientation at a time instance to another orientation shortly after. This is presented using unit quaternions. [Wertz [1994]]

Let the orientation of the spacecraft at time t be given by the quaternion $\mathbf{q}(t)$. The later orientation at time $t + \Delta t$ can then be described as $\mathbf{q}(t + \Delta t)$. The rotation between $\mathbf{q}(t)$ and $\mathbf{q}(t + \Delta t)$ can be expressed by another quaternion $\tilde{\mathbf{q}}$:

$$\mathbf{q}(t + \Delta t) = \tilde{\mathbf{q}}\, \mathbf{q}(t). \tag{2.1}$$

With the definition of a quaternion from eq. (1.5) the relation can be rewritten as:

$$\mathbf{q}(t + \Delta t) = \underbrace{\left[\cos\frac{\Delta\phi}{2}\mathbf{E} + \sin\frac{\Delta\phi}{2}\mathbf{S}\left(\mathbf{\Omega}\right)\right]}_{\tilde{\mathbf{q}}} \mathbf{q}(t) \tag{2.2}$$

with $\mathbf{E}$ being the identity matrix and $\mathbf{S}\left(\mathbf{n}\right)$ being the skew symmetric representation of the vector of rotation, $\mathbf{\Omega}$.

The angle of rotation, $\Delta\phi$, can for small rotations be approximated to be $\mathbf{\Omega}\Delta t$. Together with the small angle approximations

- $\cos\dfrac{\Delta\phi}{2} = 1$
- $\sin\dfrac{\Delta\phi}{2} = \dfrac{\mathbf{\Omega}\Delta t}{2}$

the rotation in eq. (2.2) simplifies to become

$$\mathbf{q}(t + \Delta t) \approx \left[\mathbf{E} + \frac{1}{2}\mathbf{S}\left(\mathbf{\Omega}\right)\Delta t\right] \mathbf{q}(t) \tag{2.3}$$

where $\mathbf{S}\left(\mathbf{\Omega}\right)$ is the skew symmetric representation of the angular velocity

$$\mathbf{S}\left(\mathbf{\Omega}\right) = \begin{bmatrix} 0 & \omega_z & -\omega_y & \omega_x \\ -\omega_z & 0 & \omega_x & \omega_y \\ \omega_y & -\omega_x & 0 & \omega_z \\ -\omega_x & -\omega_y & -\omega_z & 0 \end{bmatrix} \tag{2.4}$$

The rate of change of the orientation can now be found by using

$$\dot{\mathbf{q}}(t) = \frac{\mathbf{q}(t+\Delta t) - \mathbf{q}(t)}{\Delta t} \tag{2.5}$$

and by replacing the first term in the numerator with the expression from eq. (2.3), the kinematic equation becomes

$$\dot{\mathbf{q}}(t) = \frac{1}{2}\mathbf{S}\left({}^{C}_{O}\boldsymbol{\Omega}\right)\mathbf{q}. \tag{2.6}$$

or rewritten with the quaternion spilt into the imaginary and scalar part

$$\dot{q}_4 = -\frac{1}{2}{}^{C}_{O}\boldsymbol{\Omega}\bar{\mathbf{q}} \tag{2.7}$$

$$\dot{\bar{q}} = \frac{1}{2}{}^{C}_{O}\boldsymbol{\Omega}q_4 - \frac{1}{2}{}^{C}_{O}\boldsymbol{\Omega} \times \bar{\mathbf{q}} \tag{2.8}$$

2.2 Dynamic

The dynamic equation of the satellite describes how torques relates to the angular velocity of the body. These torques could for instance be the control torques (magnetorquers, momentum wheels etc.) or disturbances (aerodynamic drag, gravitational forces etc.). [Wertz [1994]]

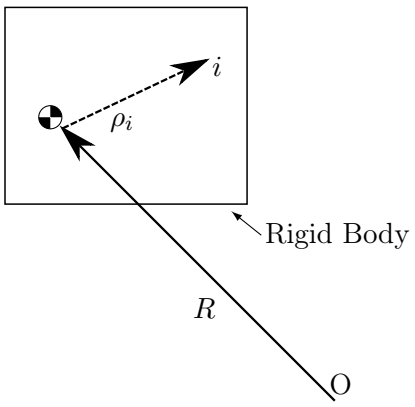

Figure 2.1: ρ_i: Vector from COM to a given mass i. R: Vector from $\mathcal{F}_r$ to COM of $\mathcal{F}_s$

The rigid body shown in figure 2.1 consists of n-mass points. From the centre of mass to the mass point i lies the vector ρ_i. The angular momentum for the rigid body rotating in the Inertial frame can by Newton's second law be defined as

$$\mathbf{L} \equiv \sum_{i=1}^{n} m_i \rho_i \times \dot{\rho}_i. \tag{2.9}$$

by rewriting $\dot{\rho_i} = \mathbf{\Omega} \times \rho_i$ and inserting it into 2.9 it becomes

$$\mathbf{L} = \sum_{i=1}^{n} m_i \rho_i \times (\mathbf{\Omega} \times \rho_i) \tag{2.10}$$

At this point the inertia is introduced. By defining the inertia as

$$I_{11} \equiv \sum_{i=1}^{n} m_i(\rho_{i2}^2 + \rho_{i3}^2) \tag{2.11a}$$

$$I_{22} \equiv \sum_{i=1}^{n} m_i(\rho_{i3}^2 + \rho_{i1}^2) \tag{2.11b}$$

$$I_{33} \equiv \sum_{i=1}^{n} m_i(\rho_{i1}^2 + \rho_{i2}^2) \tag{2.11c}$$

$$I_{21} = I_{12} \equiv -\sum_{i=1}^{n} m_i \rho_{i1} \rho_{i2} \tag{2.11d}$$

$$I_{23} = I_{32} \equiv -\sum_{i=1}^{n} m_i \rho_{i2} \rho_{i3} \tag{2.11e}$$

$$I_{31} = I_{13} \equiv -\sum_{i=1}^{n} m_i \rho_{i3} \rho_{i1} \tag{2.11f}$$

with eq. (2.11a-2.11c) being the sum of intertia and eq (2.11d-2.11f) being the product of inertia, eq. (2.10) becomes

$$\mathbf{L} \equiv \mathbf{I}_b {}_I^C\mathbf{\Omega}. \tag{2.12}$$

By letting the principal axes of the satellite form the basis for the Control frame CS, the off-diagonal elements of inertia matrix disapears, leaving only the sum of inertia on the diagonal. This is set up in matrix form as

$$\mathbf{I}_p = \begin{bmatrix} I_{11} & 0 & 0 \\ 0 & I_{22} & 0 \\ 0 & 0 & I_{33} \end{bmatrix}$$

From this, the time derivative of the angular momentum, which relates to the torques acting on the satellite, can be set up as

$$\dot{\mathbf{L}} + {}_I^C\mathbf{\Omega} \times \mathbf{L} = \mathbf{N}_{ext} \tag{2.13}$$

$$\dot{\mathbf{L}} = -{}_I^C\mathbf{\Omega} \times \mathbf{L} + \mathbf{N}_{ext} \tag{2.14}$$

with $\mathbf{N}_{ext}$ being external torques.

By rewriting eq. (2.12) to ${}_I^C\mathbf{\Omega} = \mathbf{I}_p^{-1}\mathbf{L}$, eq. (2.14) becomes

$$\dot{\mathbf{L}} = -(\mathbf{I}_p^{-1}\mathbf{L}) \times \mathbf{L} + \mathbf{N}_{ext} \tag{2.15}$$

or equivalently

$$\begin{aligned}\mathbf{I}_p {}^C_I\dot{\boldsymbol{\Omega}} &= -{}^C_I\boldsymbol{\Omega} \times (\mathbf{I}_p {}^C_I\boldsymbol{\Omega}) + \mathbf{N}_{ext} \\ {}^C_I\dot{\boldsymbol{\Omega}} &= -\mathbf{I}_p^{-1}\left[{}^C_I\boldsymbol{\Omega} \times (\mathbf{I}_p {}^C_I\boldsymbol{\Omega})\right] + \mathbf{I}_p^{-1}\mathbf{N}_{ext}.\end{aligned} \tag{2.16}$$

The external torques, $\mathbf{N}_{ext}$, is in this report set to be the input torque caused by the magnetorquers and the external torques caused by disturbances such as gravity gradient, aerodynamic drag, radiation and magnetic dipole. The selected torques are described in the next chapter.

Actuator and Disturbances 3

3.1 Magnetorquers

The satellite is controlled by six coils, mounted side by side as three pairs, placed mutually perpendicular to each other in the satellite body as seen on figure 1.1. This makes them align with the x-, y- and z-axis of the Satellite body frame respectively. When an electric current runs through these coils, a magnetic dipole moment is generated. This magnetic dipole moment can for each of the coils be described as [Hughes [2004]]

$$m = niA \tag{3.1}$$

where

- n is the windingcount of the coil
- i is the applied current
- A is the coil area.

The magnetic dipole moment from each of the coils can be combined in a vector notation. This can be written as

$${}^{S}\mathbf{m} = \begin{bmatrix} m_x \\ m_y \\ m_z \end{bmatrix} \tag{3.2}$$

As this magnetic dipole moment from the magnetorquers is given in the Satellite body frame and is needed in the Control frame, a rotation is made

$${}^{C}\mathbf{m} = {}^{C}_{S}\mathbf{A}\,{}^{S}\mathbf{m}. \tag{3.3}$$

The magnetic dipole of the magnetorquers interacts with the magnetic field from Earth, resulting in a control torque described by

$${}^{C}\mathbf{N}_{ctrl} = {}^{C}\mathbf{m} \times {}^{C}\mathbf{B} \tag{3.4}$$

$$= {}^{C}\mathbf{m} \times {}^{C}_{O}\mathbf{A}\,{}^{O}\mathbf{B} \tag{3.5}$$

where ${}^{O}\mathbf{B}$ is magnetic flux vector of Earth given in the Orbit frame. The maximal magnetic flux value from Earth can be approximated as

$$B = \frac{2M}{r^3} \tag{3.6}$$

where M is the magnetic moment of Earth and r is the distance from the centre of Earth.

The magnetorquers used in the AAUSAT project is dimentioned with the following parameters

A	Coil area	0.049	$[m^2]$
n	Coil winding count	275	$[-]$
i	Electric current	53	[mA]
r	Distance to satellite	6978	[km]
M	Earth's magnetic moment	$7.96 \cdot 10^{15}$	[T]

The magnetorquers, with the given parameters, can produce a torque of 946.46 nNm.

3.2 Gravitational Torque

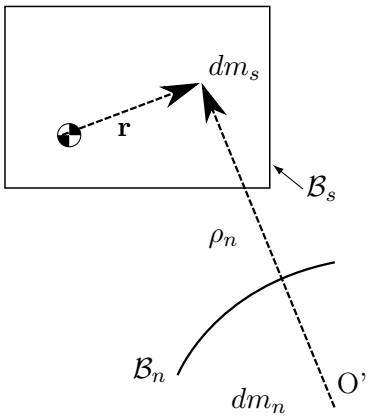

Figure 3.1: $\mathbf{r}$: Vector from COM to a given mass i. ρ_n: Vector from COM in $\mathcal{F}_r$ to m_i in $\mathcal{F}_s$

The forces acting on a mass element in the satellite body caused by the gravitational gradient from Earth can be written as [Hughes [2004]]

$$\mathrm{d}\mathbf{F}_i = \frac{-\mu \mathbf{R}_i \mathrm{d}m_i}{R_i^3} \tag{3.7}$$

with

- $\mathbf{F}_i$ being the i'th gravitational force
- μ being the gravitational constant from Earth
- $\mathbf{R}_i$ being the orientation from Earth's geocenter to the i^{th} mass element.
- R_i being the distance from the geocenter of Earth to the i^{th} mass element

The torque acting on the satellite from the gravity gradient forces becomes

$$\mathrm{d}\mathbf{N}_i = \mathbf{r}_i \times \mathrm{d}\mathbf{F}_i \tag{3.8}$$

where $\mathbf{r}_i$ is the vector from the centre of mass to the i^{th} mass element with the corresponding force $\mathbf{F}_i$.

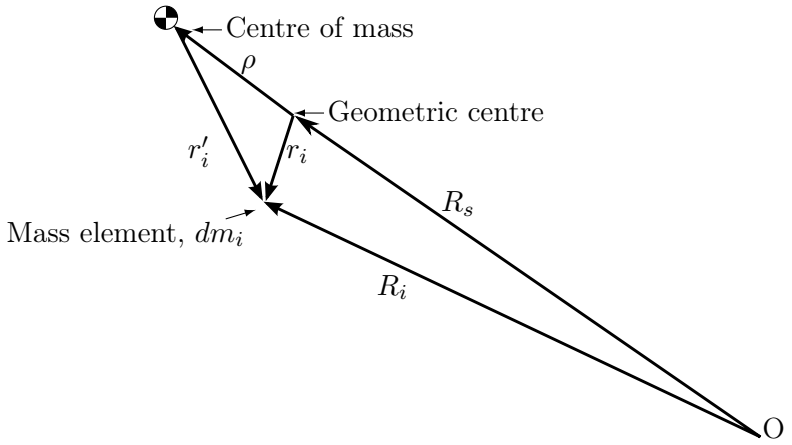

Figure 3.2: Gravity gradient torque description

The combined torque from all of the element masses can be combined as

$$\mathbf{N}_g = \int \mathbf{r}_i \times \mathrm{d}\mathbf{F}_i = \int \left(\rho + \mathbf{r}_i'\right) \times \frac{-\mu \mathbf{R}_i}{R_i^3} \mathrm{d}m_i \tag{3.9}$$

with the terminology given in figure 3.2.

Assuming that the geometric center is the centre of mass, the distance from the Earth to the satellite is much greater than the size of the satellite and that the satellite consists of a single rigid body, eq. (3.9) becomes

$$\mathbf{N}_g = \frac{3\mu}{R_s^3} \left[\hat{\mathbf{R}}_s \times \left(\mathbf{I}_p \hat{\mathbf{R}}_s\right)\right] \tag{3.10}$$

The equation from eq. (3.10) can be rewritten to fit the coordinate systems used in this report. The unit vector pointing from Earth to the satellite body, $\hat{\mathbf{R}}_s$ is the same as the zenith vector local to the orbit position. This can be found in the transformation matrix from the Orbit frame to the Satellite body frame as described in eq. (1.13)

$$\overset{S}{O}\mathbf{A} = \begin{bmatrix} {}^S\mathbf{i}_O & {}^S\mathbf{j}_O & {}^S\mathbf{k}_O \end{bmatrix} \tag{3.11}$$

with ${}^S\mathbf{c}3_O$ being the projection of the Orbit frame z-axis onto the axes of the Satellite body frame. Inserting this notation into eq. (3.10), it becomes

$$\mathbf{N}_g = 3\omega_o^2 \left({}^S\mathbf{k}_O \times \mathbf{I}_p {}^S\mathbf{k}_O\right) \tag{3.12}$$

In order to find the worst case torque caused by gravity on the satellite, each of the concerning parameters has been set equal to the worst possible values. The worst possible gravity gradient is defined to occur wwith the centre of mass displaced 2 cm towards one of the corners of the satellite, see figure 3.3,

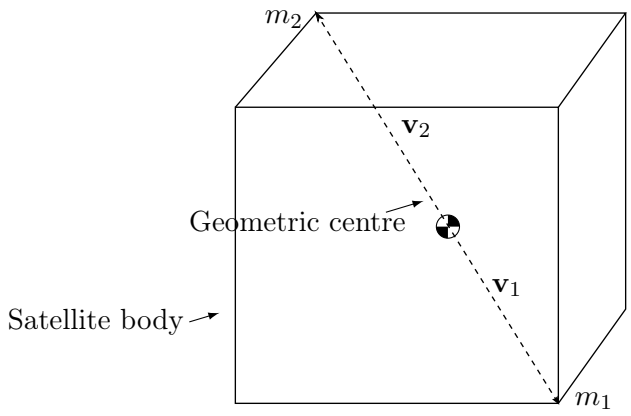

Figure 3.3: COM displacement causing maximum gravity gradient

as this increases the possibility to locate the point mass further away from the centre of mass.

The displacement of the centre of mass gives rise to a torque around the geometric centre. By calculating the distance from centre of mass to the corners and the corresponding masses, as seen on figure 3.3, the inertia matrix for the Satellite body frame can be recalculated according to eq. (2.11a - 2.11f).

Denote the vector from centre of mass to the nearest corner of the satellite by $\mathbf{v}_1$ and the opposite vector from the centre of mass to the far-off corner by $\mathbf{v}_2$, and the corresponding masses in these directions by m_1 and m_2 respectively. The new inertia matrix becomes

$$ {}^{s}\mathbf{I} = \begin{bmatrix} 0.0041 & -0.0024 & -0.0024 \\ -0.0024 & 0.0041 & -0.0024 \\ -0.0024 & -0.0024 & 0.0041 \end{bmatrix} \tag{3.13} $$

with

$$ \mathbf{v}_1 = \begin{bmatrix} 0.0385 \\ 0.0385 \\ 0.0385 \end{bmatrix} \qquad \mathbf{v}_2 = \begin{bmatrix} 0.0615 \\ 0.0615 \\ 0.0615 \end{bmatrix} $$

$$ m_1 = 0.385\,\text{kg} \qquad m_2 = 0.615\,\text{kg} \qquad |\,\mathbf{v}_1\,| = 0.0666\,\text{m} \qquad |\,\mathbf{v}_2\,| = 0.1066\,\text{m} $$

This results in a worst case gravity gradient torque of 23.98 nNm.

3.3 Aerodynamic Drag

The aerodynamic drag is caused by the surrounding atmosphere acting as a resisting force on the satellite body. The most important parameters are the area of the body drifting through the wind, and the atmospheric density. The

maximal disturbing torque caused by drag, is found when the exposed area is at its maximum and the vector from the centre of pressure to the centre of mass is perpendicular to the velocity vector, see figure 3.4. The maximum area is given as the attitude where a corner of the satellite is pointing in the orbit direction. The minimum area is given as the attitude where a side of the satellite is pointing in the orbit direction, see figure 3.5

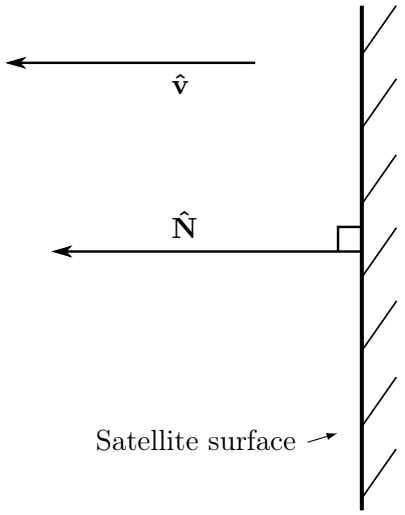

Figure 3.4: Satellite surface cutting through the wind

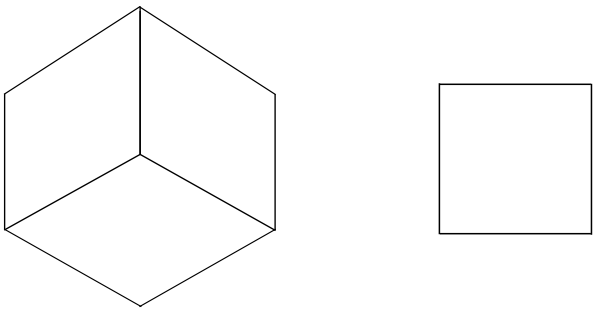

Figure 3.5: Maximum and minimum surface area

The force created by the aerodynamic drag can be calculated by the formula [Hughes [2004]]

$$\mathbf{F}_{aero} = {}^{-1}/_{2} C_D \rho \mathbf{v}^2 \left(\hat{\mathbf{N}} \cdot \hat{\mathbf{v}} \right) \hat{\mathbf{v}} \mathrm{d}A \tag{3.14}$$

with

- C_D, drag coefficient
- ρ, air density
- $\mathbf{v}$, velocity

- $\left(\hat{\mathbf{N}} \cdot \hat{\mathbf{v}}\right) \hat{\mathbf{v}}$, angle between the normal vector of the exposed area and the velocity vector
- $\mathrm{d}A$ exposed area

In these calculations, the exposed area is calculated in the direction of the velocity vector, which simplifies the formula. The resulting torque based on this force is calculated as

$$\mathbf{N}_{aero} = \mathbf{F}_{aero} \times \mathbf{R}_{com}. \tag{3.15}$$

With the following values

C_D	Drag coefficient	2	[–]
ρ_{600}	Air density at 600 km altitude	$1.454 \cdot 10^{-13}$	$[\mathrm{kg/m^3}]$
$\mathbf{v}$	Velocity	6000	[m/s]
A	Area	0.01733	$[\mathrm{m^2}]$

the worst case aerodynamic torque disturbance is calculated to be 22.54 nNm in an orbit height of 600 km. As the height decreases, the aerodynamic force, and thereby torque, increases.

3.4 Magnetic Residual Dipole

Placed in LEO, the satellite will interact with Earths magnetic field, and any magnetic field created in the satellite by electric currents or material properties will thereby result in a force in a given direction. This magnetic field strength and direction is very hard to determine prior to launching the satellite, which is why a worst case estimate is used in the following.

The satellite has been estimated as a magnetic dipole with a dipole moment of 10 $\mathrm{mAm^2}$ based on [NASA [1969]]. Like magnetorquers, the torque produced by the magnetic residual dipole disturbance can be calculated as [Wertz [1994]]

$$\mathbf{N}_{mag} = \mathbf{m}_{mag} \times \mathbf{B} \tag{3.16}$$

with $\mathbf{m}_{mag}$ being the magnetic moment of the satellite and $\mathbf{B}$ being the magnetic flux vector from Earth.

The maximal magnetic flux value from Earth can be approximated as

$$B = \frac{2M}{r^3} \tag{3.17}$$

where M is the magnetic moment of Earth and r is the distance from the centre of Earth.

Using the values from the following table, the worst case disturbing magnetic residual torque is calculated to be 468.54 nNm.

M	Earth's magnetic moment	$7.96 \cdot 10^{15}$	[T]
r	Distance from entre of Earth to satellite	6978	[km]
D	Satellite dipole moment (estimate)	10	$[\mathrm{mAm^2}]$

3.5 Solar Radiation

The light rays, mainly from the sun, that reaches the satellite will either be absorbed or reflected. In both situations the light rays will cause a pressure on the satellite body resulting in a torque around the centre of mass. The light emission and reflection from Earth and the moon could also cause a pressure on the satellite, however, this radiation is small compared to that caused by the sun.

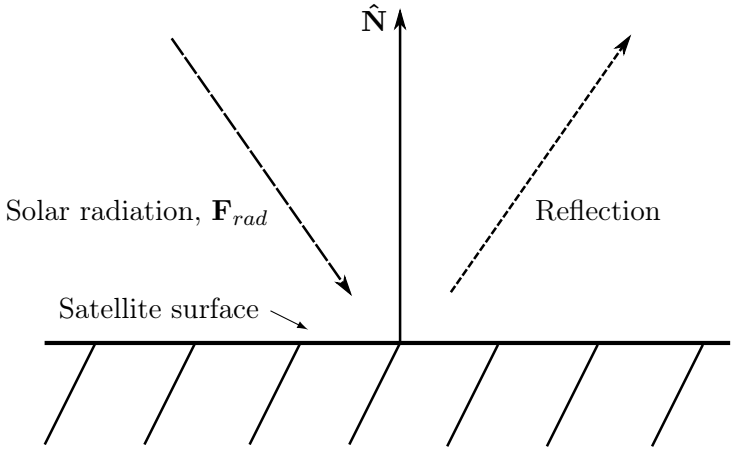

Figure 3.6: Solar radiation and reflection on satellite surface

The pressure, F_{rad}, on a radiated area is given as [Wertz [1994]]

$$F_{rad} = C_a P A \tag{3.18}$$

where C_a is the absorption constant of the radiated area, P is the solar flux and A is the radiated area. The radiation constant C_a is a number between 1 (total absorption) and 2 (total reflection).

The solar flux depends on the distance from the sun and is therefor near independent of orbit altitude in LEO. The solar flux is calculated as

$$P = \frac{F_s}{c} = 4,53 \cdot 10^{-6} \text{ kg/ms}^2 \tag{3.19}$$

with F_s being the mean solar energy, $1358\,\text{W/m}^2$, and c being the speed of light.

The resulting torque around the centre of mass is the given as

$$\mathbf{N}_{rad} = \mathbf{F}_{rad} \times \mathbf{R}_{COM} \tag{3.20}$$

where $\mathbf{R}_{COM}$ is the vector from the centre of mass to the geometric centre of radiation pressure.

The worst case torque caused by radiation can now be calculated to be 3.138 nNm, with

C_a	Absorption constant	2	[–]
P	Solar flux	$4.53 \cdot 10^{-6}$	$[^{kg}/_{ms^2}]$
A	Maximum radiated area	0.01733	$[m^2]$
$\mathbf{R}_{COM}$	Distance from geometric center to COM	2	[cm]

3.6 Disturbance Comparison

The mentioned actuator- and disturbance torques are given in the following table

	Actuator		
$\mathbf{N}_{torque}$	Magnetorquers	946.46	[nNm]
	Disturbances		
$\mathbf{N}_g$	Gravity gradient	23.98	[nNm]
$\mathbf{N}_{aero}$	Aerodynamic drag	19.26	[nNm]
$\mathbf{N}_{mag}$	Magnetic residual dipole	468.54	[nNm]
$\mathbf{N}_{rad}$	Solar radiation	3.14	[nNm]
	Resulting torque		
$\mathbf{N}_{result}$	Resulting torque	411.89	[nNm]

As seen, the most significant disturbance is by far the magnetic residual dipole, however, this is based on an estimate of the magnetic dipole moment of the satellite.

Earth's Magnetic Field and Controllability

4

Actuating the satellite by magnetorquers in Low Earth Orbit causes som challenges, as the satellite will not have full controllability.

4.1 Geomagnetic Field of Earth

The geomagnetic field surrounding Earth vary in field strength and direction according to the local position of the satellite in orbit. The magnetic field can be compared to that of a dipole magnet where the dipoles are located at the magnetic poles of Earth.

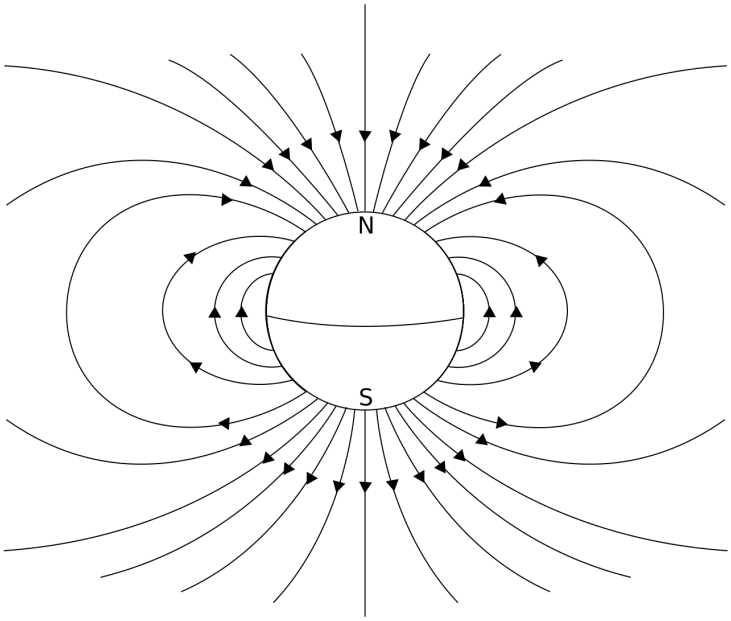

Figure 4.1: Magnetic field around Earth as a dipole. Figure provided by Wikimedia Commons

The magnetic field can be represented by the IGRF (International Geomagnetic Reference Field) model, a model approximating the magnetic field strength and direction at any location around Earth, taking the abnormalities from an ideal magnetic dipole field into account. An example of the field strength approximated by the IGRF-11 model can be seen in figure 4.2.

The magnetic field strength and direction will vary highly according to the location of the satellite. In figure 4.3 an example of an orbiting satellite is seen.

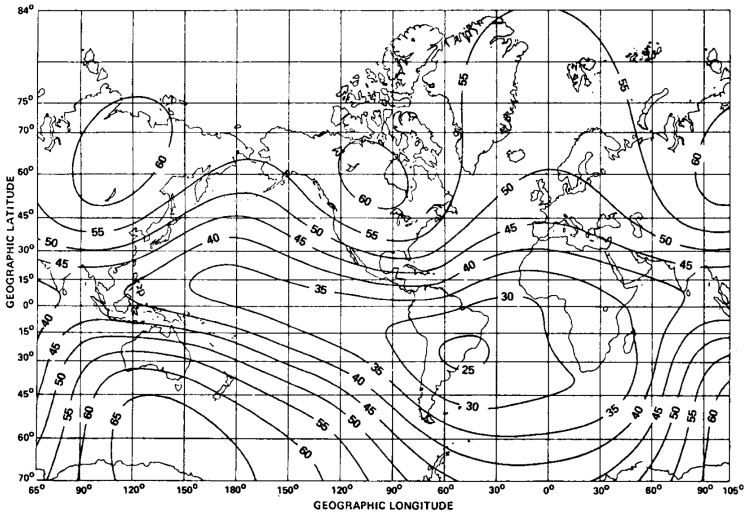

Figure 4.2: IGRF model showing field strength abnormalities [Wertz [1994]]

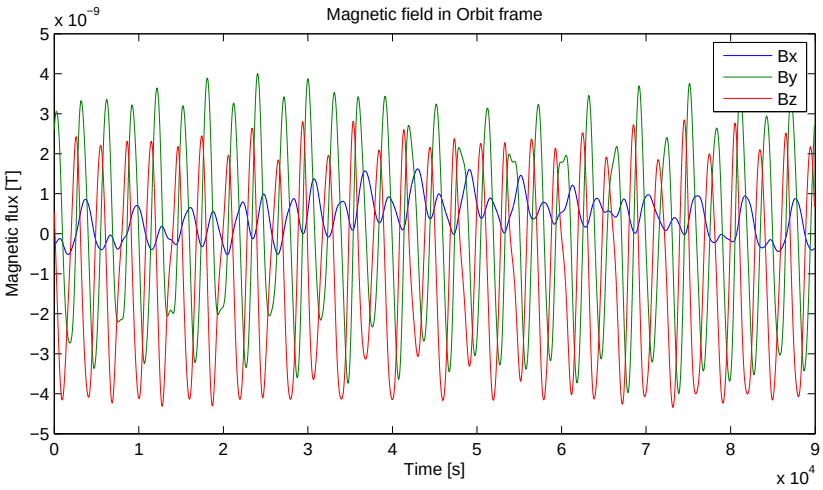

Figure 4.3: Magnetic field experienced by satellite in LEO.

4.2 Controllability

The satellite will not experience controllability in all three axes at the same time, as the torque produced by the magnetorquers can only be applied perpendicular to the direction of the magnetic field. In other words, the torque produced in a three dimensional space by the magnetorquers will be projected down onto the two dimensional plane perpendicular to the local geomagnetic field as seen on figure 4.4.

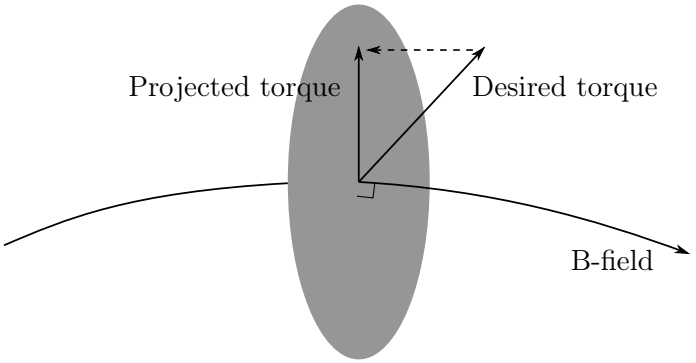

Figure 4.4: Desired torque projected down onto the plane perpendicular to the B-field

The torque produced by the magnetorquers is written as

$$\mathbf{N}_{des} = \mathbf{m} \times \mathbf{B} \tag{4.1}$$

where $\mathbf{m}$ is the magnetic dipole moment produced by the torquers $[m_x \quad m_y \quad m_z]^\intercal$ and $\mathbf{B}$ is the geomagnetic field from Earth $[B_x \quad B_y \quad B_z]^\intercal$.

The torque projected down onto the perpendicular plane can be written as [R. Wisniewski [1996]]

$$\mathbf{N}_{ctrl} = \underbrace{\left[\frac{\mathbf{N}_{des} \times \mathbf{B}}{||^C\mathbf{B}||^2}\right]}_{\mathbf{m}_{\text{projected}}} \times \mathbf{B} \tag{4.2}$$

If the desired torque is parallel to the local geomagnetic field, the resulting control torque from eq. (4.2) becomes zero. If the desired torque is perpendicular to the local geomagnetic field, the resulting- and desired torque will remain the same.

Part III

Estimation and Control

Satellite Energy and Lyapunov Stability

5

In order to prove stability for the controller in chapter 7, the Lyapunov condition is investigated in the following chapter.

An initial Lyapunov candidate is set up based on the energy of the satellite. In the following section the energy of the system is investigated, and in the subsequent sections a Lyapunov candidates for the controller is shown.

5.1 System Energy

The energy of the satellite is split into two; a kinetic energy caused by the satellite rotating between the Inertial frame and Orbit frame, and a potential energy caused by the gravity gradient and the fact that the satellite rotates around Earth, named the gyro effect. [Hughes [2004]]

Kinetic Energy

The kinetic energy is a result of the satellite rotating in the Inertial frame. The angular velocity of the satellite can be considered as a sum from the Inertial frame to the Orbit frame and the angular velocity from Orbit frame to the Satellite Reference frame. Expecting the angular velocity from the Inertial frame to the Orbit frame, ω_o, to be constant[1], the resulting expression for the kinetic energy becomes

$$E_{kinetic} = \frac{1}{2} {}^C_O\boldsymbol{\Omega}^\intercal \mathbf{I} {}^C_O\boldsymbol{\Omega} \tag{5.1}$$

Potential Energy

The potential energy is based on the effects of the gravity gradient and the rotational motion of the satellite.

The potential energy due to the gravity gradient can be written as

$$E_{gravity} = \frac{3}{2}\omega_o^2 {}^C\mathbf{k}_O \mathbf{I}_p {}^C\mathbf{k}_O \tag{5.2}$$

where ${}^C\mathbf{k}_O$ is the local Zenith unit vector resolved in the Control Reference frame.

The rotational motion of the satellite also causes a potential energy. The summand ${}^C_I\boldsymbol{\Omega} \times \mathbf{I}_p {}^C_I\boldsymbol{\Omega}$ in the dynamic model from eq. (2.16) can be rewritten according to

$${}^C_I\boldsymbol{\Omega} = {}^C_O\boldsymbol{\Omega} + \omega_o \, {}^C\mathbf{j}_O \tag{5.3}$$

[1] For a circular orbit

Only a single part of the rewritten expression contributes to the potential energy, making the potential energy due to the rotational motion become

$$E_{gyro} = -\frac{1}{2}\omega_o^{2C}\mathbf{j}_O{}^{\intercal}\mathbf{I}_p{}^{C}\mathbf{j}_O \tag{5.4}$$

Combined Energy

The combined energy for the satellite orbiting Earth can be written as

$$\begin{aligned} E_{total} &= E_{kinetic} + E_{gravity} + E_{gyro} \\ &= \frac{1}{2}{}^{C}_{O}\mathbf{\Omega}^{\intercal}\mathbf{I}^{C}_{O}\mathbf{\Omega} + \frac{3}{2}\omega_o^{2C}\mathbf{k}_O\mathbf{I}_p{}^{C}\mathbf{k}_O - \frac{1}{2}\omega_o^{2C}\mathbf{j}_O{}^{\intercal}\mathbf{I}_p{}^{C}\mathbf{j}_O \end{aligned} \tag{5.5}$$

5.2 Lyapunov Stability

The controller described in the following chapters can be proven stable by looking at a Lyapunov candidate function (LCF). The LCF can tell if the controller is stable or asymptotically stable. It is necessary to point out that a LCF is only a sufficient condition for the controller to be stable; if the conditions for the LCF are not satisfied for a specific controller it does not mean that the controller is unstable.

From Khalil [2002] the LCF can be defined as:

Let $x = 0$ be an equilibrium point for $\dot{x} = f(x)$ and $D \subset R^n$ be a domain containing $x = 0$. Let $V : D \rightarrow R$ be a continuously differentiable function such that

$$V(0) = 0 \quad \text{and} \quad V(x) > 0 \text{ in } D - \{0\} \tag{5.6}$$

$$\dot{V}(x) \leq 0 \quad \text{in} \quad D \tag{5.7}$$

Then, $x = 0$ is stable. Moreover, if

$$\dot{V}(x) < 0 \quad \text{in} \quad D - \{0\} \tag{5.8}$$

then $x = 0$ is asymptotically stable.

Energy Based LCF

As the behavior of the Lyapunov candidate function is coinciding with the desired properties of the energy of a stable system, an initial guess for a LCF to prove stability for a controller would be based on the energy expression from eq. (5.5)

$$
\begin{aligned}
V &= E_{total} \\
&= \frac{1}{2}{}^{C}_{O}\boldsymbol{\Omega}^{\intercal}\mathbf{I}^{C}_{O}\boldsymbol{\Omega} + \frac{3}{2}\omega_o^{2C}\mathbf{k}_O\mathbf{I}_p{}^{C}\mathbf{k}_O - \frac{1}{2}\omega_o^{2C}\mathbf{j}_O{}^{\intercal}\mathbf{I}_p{}^{C}\mathbf{j}_O
\end{aligned} \tag{5.9}
$$

The derivative of the LCF can be written as

$$
\dot{V} = {}^{C}_{O}\boldsymbol{\Omega}^{\intercal}\mathbf{I}^{C}_{O}\dot{\boldsymbol{\Omega}} + 3\omega_o^{2C}\mathbf{k}_O\mathbf{I}_p{}^{C}\dot{\mathbf{j}}_O - \omega_o^{2C}\mathbf{j}_O{}^{\intercal}\mathbf{I}_p{}^{C}\dot{\mathbf{j}}_O \tag{5.10}
$$

From the system dynamics, an expression for $\mathbf{I}_{pO}^{C}\dot{\boldsymbol{\Omega}}$ can be obtained by using eq. (5.3)

$$
\begin{aligned}
\mathbf{I}_{pO}^{C}\dot{\boldsymbol{\Omega}} = \omega_o^2\mathbf{I}_p{}^{C}\dot{\mathbf{j}}_O - \mathbf{S}\left[{}^{C}_{O}\boldsymbol{\Omega}\right]\mathbf{I}_{pO}^{C}\boldsymbol{\Omega} + \omega_o^2\mathbf{S}\left[{}^{C}_{O}\boldsymbol{\Omega}\right]\mathbf{I}_p{}^{C}\mathbf{j}_O + \omega_o^2\mathbf{S}\left[{}^{C}_{O}\boldsymbol{\Omega}\right]\mathbf{I}_{pO}^{C}\boldsymbol{\Omega} \\
- \omega_o^2\mathbf{S}\left[{}^{C}\mathbf{j}_O\right]\mathbf{I}_p{}^{C}\mathbf{j}_O + \underbrace{3\omega_o^2\mathbf{S}\left[{}^{C}\mathbf{k}_O\right]\mathbf{I}_p{}^{C}\mathbf{k}_O}_{\mathbf{N}_{gg}} + \mathbf{N}_{ctrl}
\end{aligned} \tag{5.11}
$$

The LCF derivative can be reduced by inserting eq. (5.11) into eq. (5.10) and use the following math operators

$$
{}^{C}_{O}\boldsymbol{\Omega}\ \ \mathbf{S}\left[{}^{C}_{O}\boldsymbol{\Omega}\right] = 0 \tag{5.12}
$$

$$
{}^{C}\dot{\mathbf{j}}_O = \mathbf{S}\left[{}^{C}\mathbf{j}_O\right]{}^{C}_{O}\boldsymbol{\Omega} \tag{5.13}
$$

$$
{}^{C}_{I}\dot{\boldsymbol{\Omega}} = {}^{C}_{O}\dot{\boldsymbol{\Omega}} + \omega_o\mathbf{S}\left[{}^{C}\mathbf{j}_O\right]{}^{C}_{O}\boldsymbol{\Omega} \tag{5.14}
$$

The LCF derivative now becomes

$$
\begin{aligned}
\dot{V} = {}^{C}_{O}\boldsymbol{\Omega}^{\intercal}\Big[\omega_o^2\mathbf{I}_p{}^{C}\dot{\mathbf{j}}_O - \mathbf{S}\left[{}^{C}_{O}\boldsymbol{\Omega}\right]\mathbf{I}p_{O}^{C}\boldsymbol{\Omega} + \omega_o^2\mathbf{S}\left[{}^{C}_{O}\boldsymbol{\Omega}\right]\mathbf{I}_p{}^{C}\mathbf{j}_O + \omega_o^2\mathbf{S}\left[{}^{C}_{O}\boldsymbol{\Omega}\right]\mathbf{I}_{pO}^{C}\boldsymbol{\Omega} - \\
\omega_o^2\mathbf{S}\left[{}^{C}\mathbf{j}_O\right]\mathbf{I}_p{}^{C}\mathbf{j}_O + 3\omega_o^2\mathbf{S}\left[{}^{C}\mathbf{k}_O\right]\mathbf{I}_p{}^{C}\mathbf{k}_O + \mathbf{N}_{ctrl}\Big] + 3\omega_o^{2C}\mathbf{k}_O\mathbf{I}_p{}^{C}\dot{\mathbf{k}}_O - \omega_o^{2C}\mathbf{j}_O{}^{\intercal}\mathbf{I}_p{}^{C}\dot{\mathbf{j}}_O
\end{aligned} \tag{5.15}
$$

$$
\dot{V} = {}^{C}_{O}\boldsymbol{\Omega}^{\intercal}\mathbf{N}_{ctrl} \tag{5.16}
$$

It will later be shown that the energy based LCF can not be used to prove asymptotic stability for the Sliding Mode Controller in chapter 7, however it can be used to prove other attitude controllers asymptotically stable. Another attempt to make a LCF is shown in the following section.

Additional LCF

To prove stability for the Sliding Mode Controller, another LCF is set up. The energy based LCF fails the condition of $\dot{V}(x) \leq 0$ for the SMC; a condition which is belived possible to meet with another LCF. [R. Wisniewski [1996]]

It will be shown in chapter 7 that a desirable LCF derivative could look like

$$\dot{V} = \bar{\mathbf{q}}^{\intercal}{}_{O}^{C}\boldsymbol{\Omega} \tag{5.17}$$

since this can be shown to be negative definite. From the kinematics, the derivative of the real part of the quaternion is

$$\dot{q}_4 = -\frac{1}{2}{}_{O}^{C}\boldsymbol{\Omega} \cdot \bar{\mathbf{q}} \tag{5.18}$$

A LCF that supports this derivative can be written as

$$V = 2(1 - q_4) \tag{5.19}$$

or equivalent, by the expression $\bar{\mathbf{q}}\intercal\,\bar{\mathbf{q}} + q_4^2 = 1$, as

$$V = \bar{\mathbf{q}}^{\intercal}\bar{\mathbf{q}} + (1 - q_4)^2 \tag{5.20}$$

Magnetic Dipole Moment Estimation

6

From chapter 2 it was shown, based on an estimate, that the magnetic dipole moment of the satellite was the largest disturbance by far. In order for the attitude controller to counteract this magnetic dipole moment, an estimation is necessary.

From the disturbance comparison made earlier it was seen, that the magnetic dipole moment of the satellite was by far the greatest. In order to make a precise estimation of the magnetic dipole moment, a method using an Extended Kalman Filter (EKF) is proposed in the following. [T. Inamori [2010]]

6.1 Estimation Method

The proposed method for estimating the magnetic dipole moment is based on augmenting an Extended Kalman Filter (EKF) as it could be considered a traditional bias estimation. The dynamic model for the system relates the external torques to the behavior of the satellite, as was described in section 2.2. By letting the satellite perform without input control in detumbled mode the only torques acting on the satellite is the disturbances described in chapter 3. The estimation requires knowledge about the change in angular velocity measured by the gyroscopes, and the magnetic field around the satellite measured by the magnetometers.

6.2 Magnetic Dipole Estimation

The estimation of the magnetic dipole moment is made with an augmented EKF. An EKF is chosen over a traditional (linear) Kalman filter, as this offers the possibility to linearize the system at all time instances. As the magnetic field from Earth is part of the system equation, this is highly desired.

The estimation consists of two parts; a prediction- and an update part. The prediction step uses the previous state estimate together with the system model to calculate a new state estimate. The update step uses the state prediction together with a measurement to create the resulting state estimate. For some applications, multiple prediction steps may be performed per update step, or likewise the other way around.

The EKF is operating in discrete time where the system model is given as

$$\mathbf{x}_k = \mathbf{\Phi}_k \mathbf{x}_{k-1} + \mathbf{\Gamma}_k \mathbf{u}_k + \mathbf{G}_k \mathbf{w}_k \tag{6.1}$$

$$\mathbf{z}_k = \mathbf{H}_k \mathbf{x}_k + \mathbf{D}_k \mathbf{u}_k + \mathbf{v}_k \tag{6.2}$$

As mentioned earlier, the control input is set to zero in this application,

reducing eq. (6.1 - 6.2) to

$$\mathbf{x}_k = \mathbf{\Phi}_k \mathbf{x}_{k-1} + \mathbf{G}_k \mathbf{w}_k$$
$$\mathbf{z}_k = \mathbf{H}_k \mathbf{x}_k + \mathbf{v}_k$$

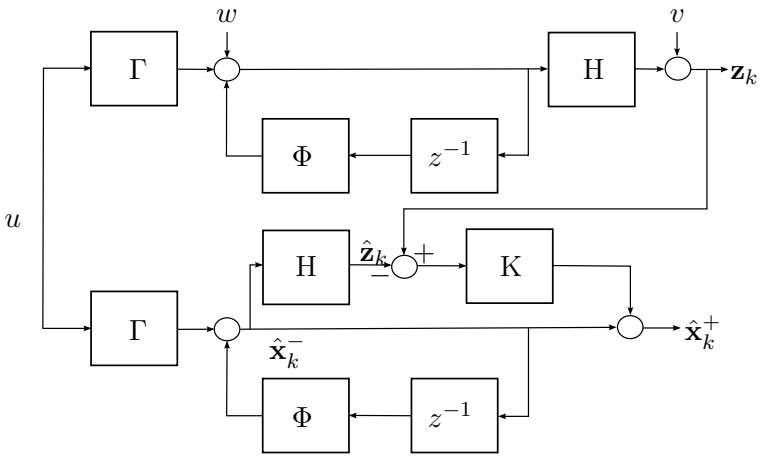

Figure 6.1: Kalman filter

From figure 6.1 the structure of the Kalman Filter can be seen as a traditional observer. This leads to the following equations for the EKF predict- and update part [M. Grewal and A. Andrews [2008]]

Prediction

$$\hat{\mathbf{x}}_k^- = \mathbf{\Phi}_k \hat{\mathbf{x}}_{k-1}^+ \tag{6.3}$$
$$\hat{\mathbf{z}}_k = \mathbf{H}_k \hat{\mathbf{x}}_k^- \tag{6.4}$$
$$\mathbf{P}_k^- = \mathbf{\Phi}_k \mathbf{P}_{k-1}^+ \mathbf{\Phi}_k^\intercal + \mathbf{Q}_{k-1} \tag{6.5}$$

Update

$$\mathbf{K}_k = \mathbf{P}_k^- \mathbf{H}_k^\intercal \left(\mathbf{H}_k \mathbf{P}_k^- \mathbf{H}_k^\intercal + \mathbf{R}_k \right)^{-1} \tag{6.6}$$
$$\hat{\mathbf{x}}_k^+ = \hat{\mathbf{x}}_k^- + \mathbf{K}_k \left(\mathbf{z} - \hat{\mathbf{z}} \right) \tag{6.7}$$
$$\mathbf{P}_k^+ = \left(\mathbf{E} - \mathbf{K}_k \mathbf{H}_k \right) \mathbf{P}_k^- \tag{6.8}$$

The dynamical model for the satellite is used in the EKF, as this relates the input torques to the angular velocities as mentioned earlier. The dynamical model has been given in eq. (2.16) as (with frames omitted)

$$\mathbf{I}_p \Delta \dot{\mathbf{\Omega}} = -\mathbf{\Omega} \times (\mathbf{I}_p \mathbf{\Omega}) + \mathbf{m} \times \mathbf{B} \tag{6.9}$$

where all disturbances except the magnetic dipole moment has been neglected. The model is linearised according to

$$\mathbf{x} = \mathbf{x_{ref}} + \Delta \mathbf{x}. \tag{6.10}$$

where the system is to be linearised around $\mathbf{x_{ref}}$. This makes the system model become

$$\Delta\dot{\Omega} = \mathbf{I}_p^{-1}(\mathbf{S}[\mathbf{I}_p\mathbf{\Omega_{ref}}] - \mathbf{S}[\mathbf{\Omega_{ref}}]\mathbf{I}_p)\Delta\mathbf{\Omega} - \mathbf{I}_p^{-1}(\mathbf{S}[\mathbf{B}])\Delta\mathbf{m} \tag{6.11}$$

with $\mathbf{S}[\cdot]$ being a skew symmetric representation.

Since the EKF is augmented with the magnetic dipole moment, the state vector can be described as

$$\mathbf{x} = \begin{bmatrix}\mathbf{\Omega}\\ \mathbf{m}\end{bmatrix} = \begin{bmatrix}\mathbf{\Omega_{ref}}_{3\times1}\\ \mathbf{m_{ref}}_{3\times1}\end{bmatrix} + \begin{bmatrix}\Delta\mathbf{\Omega}_{3\times1}\\ \Delta\mathbf{m}_{3\times1}\end{bmatrix} \tag{6.12}$$

with $\mathbf{\Omega} = [\omega_x \quad \omega_y \quad \omega_z]^\intercal$ being the angular velocities and $\mathbf{m} = [m_x \quad m_y \quad m_z]^\intercal$ being the magnetic dipole moment given in the Satellite reference frame.

The EKF uses the following dimensions and values for the calculations

$$\mathbf{A} = \begin{bmatrix}\mathbf{I}^{-1}(\mathbf{S}[\mathbf{I}\mathbf{\Omega}_{ref}] - \mathbf{S}[\mathbf{\Omega}]\mathbf{I}) & \mathbf{S}[-\mathbf{I}^{-1}\mathbf{B}]\\ \mathbf{0}_{3\times3} & \mathbf{0}_{3\times3}\end{bmatrix} \tag{6.13}$$

$$\mathbf{B} = \begin{bmatrix}\mathbf{E}_{6\times6}\end{bmatrix} \tag{6.14}$$

$$\mathbf{H} = \begin{bmatrix}\mathbf{E}_{3\times3} & \mathbf{0}_{3\times3}\end{bmatrix} \tag{6.15}$$

$$\mathbf{Q} = \begin{bmatrix}\mathbf{E}_{3\times3} & \mathbf{0}_{3\times3}\\ \mathbf{0}_{3\times3} & 10^{-3}\cdot\mathbf{E}_{3\times3}\end{bmatrix} \tag{6.16}$$

$$\mathbf{R} = 10^{-1}\cdot\begin{bmatrix}\mathbf{E}_{3\times3}\end{bmatrix} \tag{6.17}$$

The above dimensions and values have been used in simulations to test the EKF performance. In the following sections different situations are tested.

Estimation Results

Firstly the functionality of the EKF is verified by letting all the disturbances, except the satellite magnetic dipole, be set to zero and let the EKF estimate the magnetic dipole moment. For the verification simulation the following values have been used:

Maximum gravity gradient	0	Nm
Maximum aerodynamic drag	0	Nm
Maximum solar radiation	0	Nm
Magnetic residual dipole	$[0 \quad 0 \quad -0.006]^\intercal$	Am^2
Orbit height	600	km
Initial angular velocity	$10^{-3}\cdot[1 \quad 1 \quad 1]^\intercal$	rad/s
Simulation time	4	orbits

The wanted output from the EKF estimation would be the same as the set magnetic dipole moment at the simulation. An average of the last 15,000 seconds of the estimator output, as seen on figure 6.2, results in a satisfying magnetic dipole estimation of $[0 \quad 0 \quad -0.0059]^\intercal$ Am^2 .

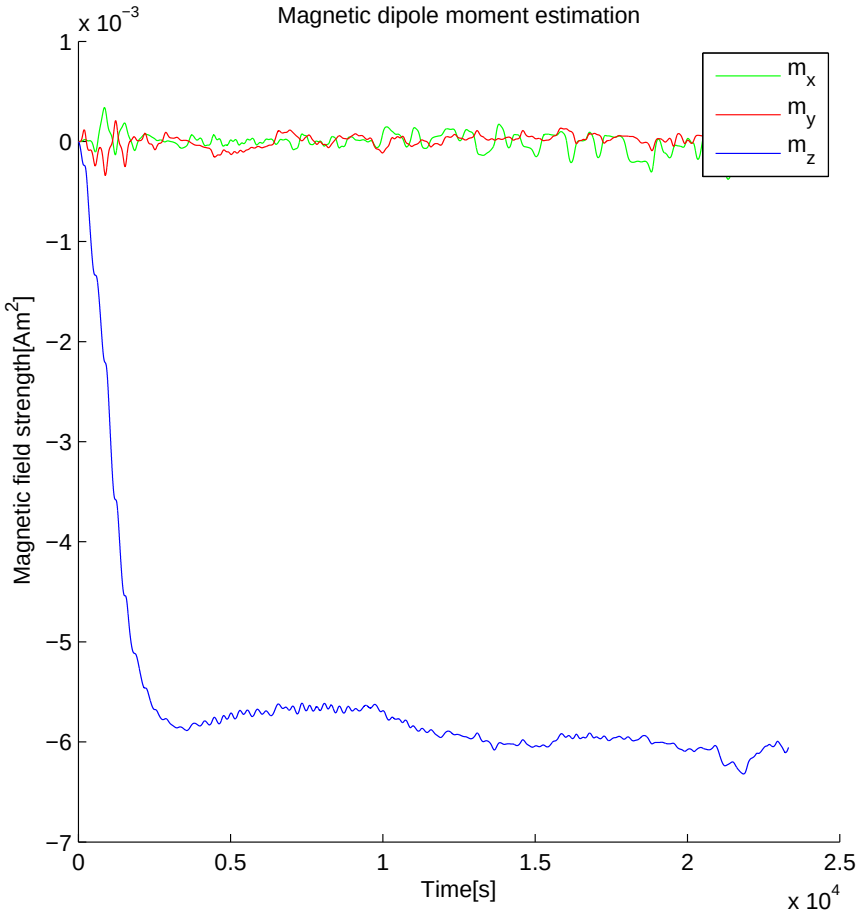

Figure 6.2: Satellite magnetic dipole estimation with EKF

Confident in the estimation results, the previously neglected disturbances have been reinserted into the simulation. The parameters for the Kalman filter has been kept the same as previously and the simulation parameters set to be the following:

Maximum gravity gradient torque	23.89	nNm
Maximum aerodynamic drag torque	19.26	nNm
Maximum solar radiation torque	31.38	nNm
Magnetic residual dipole	$[0.002 \quad -0.002 \quad -0.006]^\intercal$	Am^2
Orbit height	600	km
Initial angular velocity	$10^{-3} \cdot [1 \quad 1 \quad 1]^\intercal$	rad/s
Simulation time	4	orbits

From the results show in figure 6.3 the output average of the last 15,000 seconds results in a magnetic dipole moment estimation of $[0.0021 \quad -0.0018 \quad -0.0058]^\intercal$ Am^2.

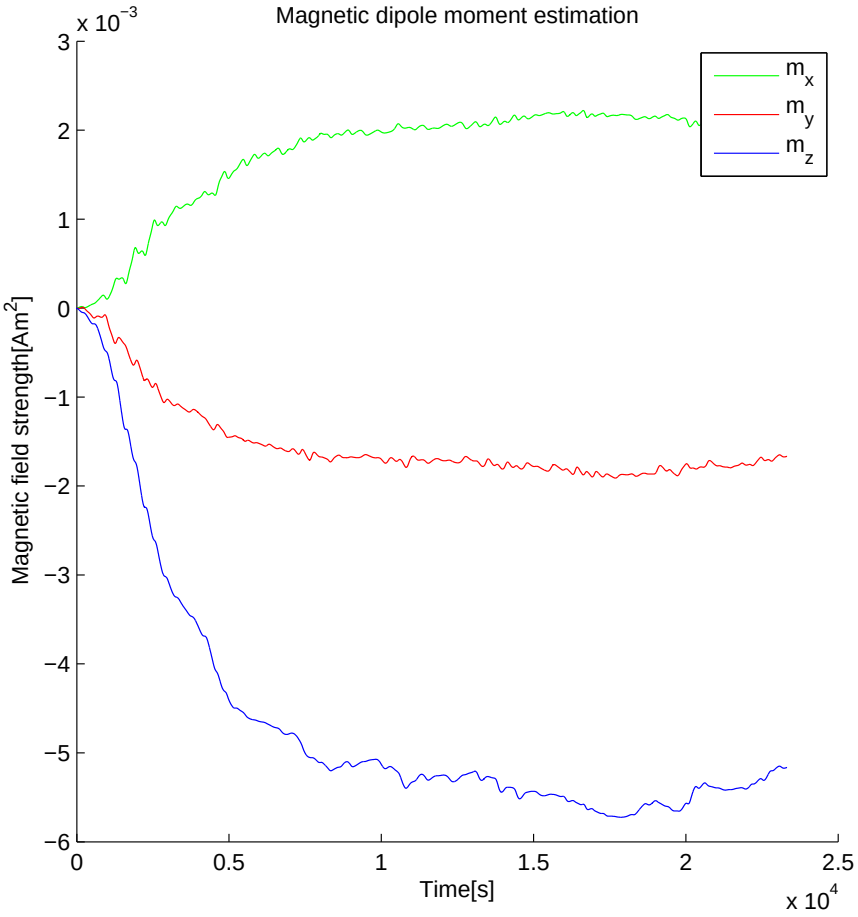

Figure 6.3: Satellite magnetic dipole estimation with EKF

Implementation Considerations

The data used for the previously calculated estimate has been captured from a simulation tool, which provided the data with a perfect state knowledge. In order to use the EKF to estimate the magnetic dipole moment of an orbiting satellite, some additional work needs to be made.

Sensor Bias

The sensors used to measure the magnetic field surrounding the satellite, magnetometer, and the angular velocity, accelerometer, needs to be calibrated in order for the measurements to be usefull. For both sensors this can be done with a least square approximation.

Estimation with State Noise

The previous estimations are based on simulation data without any noise. In the following estimation, a white noise with the variance $\sigma^2 = 0.0001$ has been included at the equation in (6.1) as $\mathbf{w}$ and a noise with variance $\sigma^2 = 0.000012$ into eq. (6.2) at $\mathbf{v}$, in order to represent the uncertainties in the measurements. These values are based on the results in [K. Vinther and K. Jensen [2010]].

The parameters have been kept the same as in the previous simulation

Maximum gravity gradient torque	23.89	nNm
Maximum aerodynamic drag torque	19.26	nNm
Maximum solar radiation torque	31.38	nNm
Magnetic residual dipole	$[0.002 \quad -0.002 \quad -0.006]^\intercal$	Am^2
Orbit height	600	km
Initial angular velocity	$10^{-3} \cdot [1 \quad 1 \quad 1]^\intercal$	rad/s
Simulation time	4	orbits

The resulting estimate from the EKF based on noisy data can be seen on figure 6.4. The average of the last 10,000 seconds is calculated to be $[0.0021 \quad -0.0017 \quad -0.0056]^\intercal$ Am^2, which correspond to an estimation error of 7.8 %.

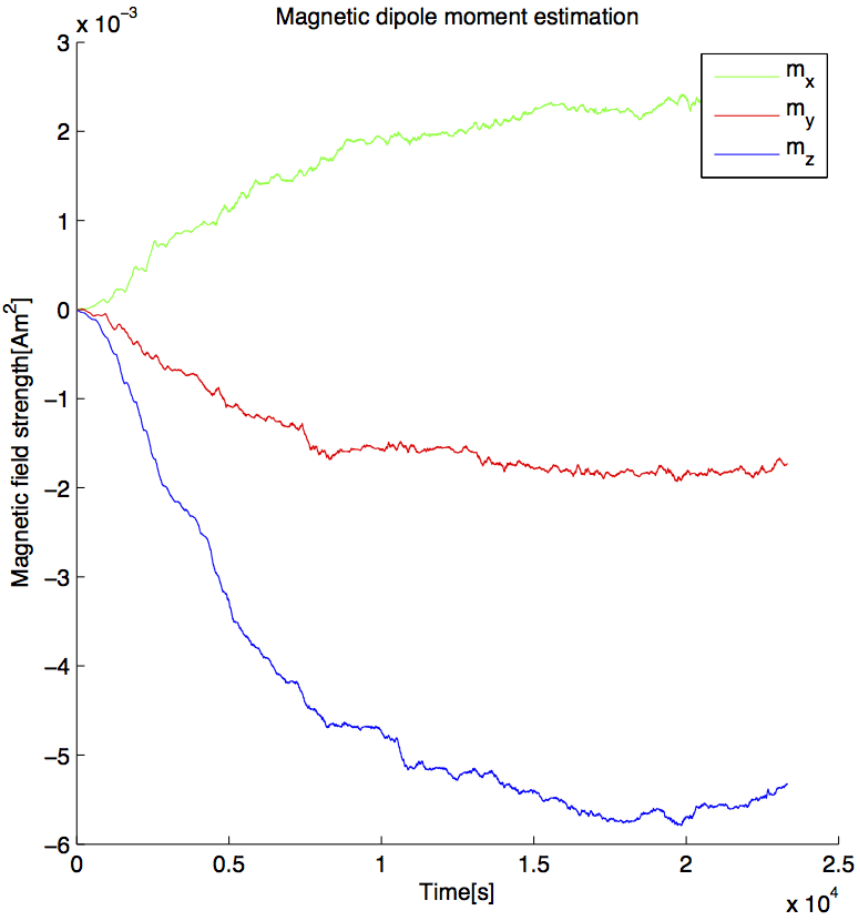

Figure 6.4: Satellite magnetic dipole estimation with EKF of noisy data.

7 Sliding Mode Controller

A non-linear attitude controller is in the following presented, as it is believed to outperform traditional linear controllers.

7.1 Sliding Mode Introduction

A Sliding Mode Controller (SMC) is chosen as the attitude controller structure for the project.

A SMC works by acting on basis of the system states. The actuations is divided into two parts, a reaching phase and a sliding phase. In the reaching phase the controller makes the system states reach a sliding manifold from an arbitrary state. The consecutive sliding phase makes the system states converge to an equilibrium by letting the states follow the sliding manifold, hence the name of the phase. These two phases can be seen in the phase portrait on figure 7.1.

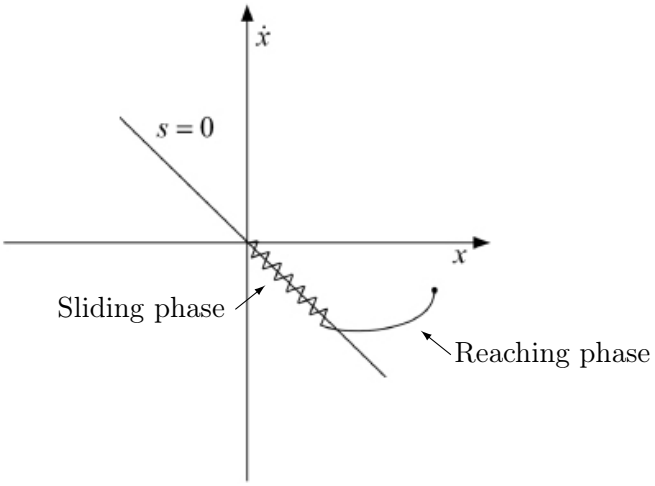

Figure 7.1: Phase portrait of a converging SMC. Illustration from [http://ej.iop.org].

The sliding- and reaching phase is defined by a variable, the sliding manifold, denoted s. The manifold is designed to ensure convergence of the system states towards an equilibrium. When the system is off the manifold, $s \neq 0$, it is said to be in the reaching phase. When the system is on the manifold, $s = 0$, the system is said to be in the sliding phase.

Reaching phase

The purpose of the reaching phase is to force the states of the system towards the sliding manifold. This is done by applying a control gain according to the position of the system states in proportion to the sliding variable.

Mathematical the reaching phase can be describes as [Bandyopadhyay [2006]]

$$\lim_{s\to 0^+} \dot{s} < 0 \qquad \lim_{s\to 0^-} \dot{s} > 0 \tag{7.1}$$

or

$$s\dot{s} < 0. \tag{7.2}$$

To make sure the system states reaches the sliding manifold in finite time, the control gain is traditionally implemented as a *sign*-function. This makes the controller act a bang-bang structure depending on the sign of s. This is written as

$$sign(s) = \begin{cases} 1 & s > 0 \\ 0 & s = 0 \\ -1 & s < 0 \end{cases} \tag{7.3}$$

To reduce chattering at the manifold, the controller could actuate on the basis of an alternative function, like the saturation function

$$sat(x) = \begin{cases} x & |x| \leq 1 \\ 0 & x = 0 \\ sign(x) & |x| > 1 \end{cases} \tag{7.4}$$

where x represents the slope $\frac{s}{\varepsilon}$.

Sliding Phase

The reaching phase is preceded by the sliding phase. This is given as the phase, where the system dynamics has reached the sliding manifold and is sliding along it towards the equilibrium. The sliding phase can be seen on figure 7.1 where the chattering around the sliding manifold is visible. This magnitude and characteristics of this chatter is decided by the structure of the sliding variable, for instance by choosing the saturation function in eq. (7.4) instead of the sign function from eq. (7.3).

Further more, the gain of the sliding variable determines how far away from the sliding manifold the system states deviates and how well it suppresses disturbances. [Khalil [2002]]

7.2 Sliding Manifold Design

The design of the SMC is divided into two, the sliding manifold and the sliding condition. Firstly the manifold is designed and in the next section the sliding condition is designed. [R. Wisniewski [1996]]

The sliding manifold has to be able to make the system converge. The equilibrium for the system operating in Nadir mode is defined between the Satellite Body frame and the Orbit frame. The velocity between the frames must be zero, ${}^S_O\boldsymbol{\Omega} = \mathbf{0}$, and the quaternion orientation must keep the frames aligned ${}^S_O\mathbf{q} = [0 \quad 0 \quad 0 \quad 1]^\intercal$. The deviation between the equilibrium and the actual states is defined as the errors, denoted $\bar{\boldsymbol{\Omega}}$ and $\bar{\mathbf{q}}$ respectively.

A Sliding Variable that makes the system converge can be set up as

$$\mathbf{s} = \bar{\boldsymbol{\Omega}} + \mathbf{K}_s\bar{\mathbf{q}} \tag{7.5}$$

where $\mathbf{K}_s$ is a positive gain constant. When the system is on the manifold, $\mathbf{s} = 0$, the sliding variable can be rewritten as

$$\bar{\boldsymbol{\Omega}} = -\mathbf{K}_s\bar{\mathbf{q}} \tag{7.6}$$

Convergence

The convergence towards the equilibrium can be proven by looking at the Luapunov Candidate Functions from chapter 5.

Energy Based LCF

The derivative of the LCF based on kinetic and potential energy from chapter 5 became:

$$\dot{V} = \bar{\boldsymbol{\Omega}}\mathbf{N}_{ctrl} \tag{7.7}$$

which, by eq. (7.6), can be rewritten as

$$\dot{V} = -\mathbf{K}_s\bar{\mathbf{q}}\mathbf{N}_{ctrl} \tag{7.8}$$

The control torque, $\mathbf{N}_{ctrl}$ can not be guaranteed to be positive definite, which is why the condition of a negative definite LCF derivative can not be fulfilled in order to achieve a asymptotically stable system. As the LCF is sufficient criterions, this failed condition does not say anything about the stability of the system. Another LCF can therefor be tested to prove asymptotical stability.

Alternative LCF

The second attempt to create a LCF in chapter 5 is tested to guarantee asymptotical stability. The LCF was given as

$$V = 2(1 - q_4) \tag{7.9}$$

$$\dot{V} = \bar{\mathbf{q}}^\intercal\bar{\boldsymbol{\Omega}} = -\bar{\mathbf{q}}^\intercal\mathbf{K}_s\bar{\mathbf{q}} \tag{7.10}$$

As $\mathbf{K}_s$ is a positive definite gain, the derivate is negative definite. The LCF therefore satisfies the criterions from section 5.2 and can be considered to be asymptotical stable.

7.3 Sliding Condition Design

The sliding condition can be understood as the control gain needed for the system to reach the sliding manifold from an arbitrary point in the space of the sliding variable. To determine the sliding condition, the sliding variable is considered. The time derivative of the sliding variable can be considered as the satellite motion on the space of the sliding variable

$$\dot{\mathbf{s}} = \overset{C}{\mathbf{O}}\dot{\mathbf{\Omega}} + \mathbf{K}_s \overset{C}{O}\dot{\mathbf{q}} \tag{7.11}$$

Eq. (7.11) can be rewritten by the dynamic and kinetic equations

$$\begin{aligned} \mathbf{I}\dot{\mathbf{s}} &= \mathbf{I}\overset{C}{I}\dot{\mathbf{\Omega}} + \mathbf{I}\mathbf{K}_s\dot{\mathbf{q}} && (7.12)\\ &= -\overset{C}{I}\mathbf{\Omega} \times (\mathbf{I}\overset{C}{I}\mathbf{\Omega}) - \omega_o \mathbf{I}({}^{C}\mathbf{j}_O \times \overset{C}{O}\mathbf{\Omega}) + \mathbf{I}\mathbf{K}_s \left[\overset{C}{O}\mathbf{\Omega} q_4 + \overset{C}{O}\mathbf{\Omega}\bar{\mathbf{q}}\right] \\ &\qquad + \mathbf{N}_{dist} + \mathbf{N}_{ctrl} && (7.13) \end{aligned}$$

The terms in eq. (7.13) can be split into two. Terms describing the motion of the satellite and a term describing the control torque applied to the satellite. If the system is on the sliding manifold, the torque needed to keep the system at the manifold can be described as the terms from eq. (7.13) regarding the satellite motion. If the system is not on the sliding manifold, a torque is needed to force the system states towards it. This torque can be terms regarding the control torque from eq. (7.13). Eq. (7.13) is therefore split into an equivalent torque and a control torque

$$\mathbf{I}\dot{\mathbf{s}} = \underbrace{-\overset{C}{I}\mathbf{\Omega} \times (\mathbf{I}\overset{C}{I}\mathbf{\Omega}) - \omega_o \mathbf{I}({}^{C}\mathbf{j}_O \times \overset{C}{O}\mathbf{\Omega}) + \mathbf{I}\mathbf{K}_s \left[\overset{C}{O}\mathbf{\Omega} q_4 + \overset{C}{I}\mathbf{\Omega}\bar{\mathbf{q}}\right] + \mathbf{N}_{dist}}_{\text{Negative equivalent torque}} \underbrace{+\mathbf{N}_{ctrl}}_{\text{Control torque}}$$

which corresponds to

$$\mathbf{N}_{eq} = \overset{C}{I}\mathbf{\Omega} \times (\mathbf{I}\overset{C}{I}\mathbf{\Omega}) + \omega_o \mathbf{I}({}^{C}\mathbf{j}_O \times \overset{C}{O}\mathbf{\Omega}) - \mathbf{I}\mathbf{K}_s \left[\overset{C}{O}\mathbf{\Omega} q_4 + \overset{C}{I}\mathbf{\Omega}\bar{\mathbf{q}}\right] - \mathbf{N}_{dist} \tag{7.14}$$

Sign-based Sliding Condition

The sliding condition used as the control torque can, according to [Bandyopadhyay [2006]], be written as

$$\mathbf{N}_{ctrl} = -\lambda sign(\mathbf{s}). \tag{7.15}$$

as it was stated in eq. (7.3). λ is a positive gain constant. This equation is only true if the system is able to actuate the control torque in any direction. This is not the case for the satellite actuated by magnetorquers, as seen in chapter 4, as the desired control torque is projected down on a two-dimensional plane perpendicular to the local magnetic field of Earth. The magnetic moment from this projection can be written as

$${}^{C}\mathbf{m} = \frac{\mathbf{N}_{\text{Desired Torque}} \times {}^{C}\mathbf{B}}{||{}^{C}\mathbf{B}||^2} \tag{7.16}$$

where the desired torque should be replaced by the sliding condition from eq. (7.15).

$$ {}^{C}\mathbf{m} = \frac{-\lambda sign(\mathbf{s})}{||{}^{C}\mathbf{B}||^2} \times {}^{C}\mathbf{B} \tag{7.17} $$

Inserting this expression for the magnetic moments into the equation for the differentiated sliding variable yields

$$ \dot{\mathbf{s}} = \left[\frac{-\lambda \mathbf{I}^{-1} sign(\mathbf{s})}{||{}^{C}\mathbf{B}||^2} \times {}^{C}\mathbf{B} \right] \times {}^{C}\mathbf{B} \tag{7.18} $$

$$ = \left[\frac{\mathbf{I}^{-1}\big({}^{C}\mathbf{B} \times -\lambda sign(\mathbf{s})\big)}{||{}^{C}\mathbf{B}||^2} \right] \times {}^{C}\mathbf{B} \tag{7.19} $$

assuming $\mathbf{N}_{eq} = 0$.

To check the stability of this sliding condition, it is tested with a Lyapunov Candidate Function. The LCF used is

$$ V = \frac{1}{2}\mathbf{s}^{\intercal}\mathbf{I}\mathbf{s} \tag{7.20} $$

Looking at the derivative of the LCF and inserting the expression from eq. (7.19) results in

$$ \dot{V} = \frac{-\lambda}{||{}^{C}\mathbf{B}||^2}\big({}^{C}\mathbf{B} \times \mathbf{s}\big)\big({}^{C}\mathbf{B} \times sign(\mathbf{s})\big) \tag{7.21} $$

Equation (7.21) can not be guaranteed to be negative (semi)definite, as the angles between $\big({}^{C}\mathbf{B} \times \mathbf{s}\big)$ and $\big({}^{C}\mathbf{B} \times sign(\mathbf{s})\big)$ might not have the same sign.

Continuous Sliding Condition

The *sign*-function from the previous mentioned sliding condition did not prove stable. An alternative function is in the following presented. [R. Wisniewski [1996]]

A continuous sliding variable is set up corresponding to the *sign*-based sliding variable from eq. (7.15)

$$ \mathbf{N}_{des} = \mathbf{N}_{eq} \underbrace{-\lambda \mathbf{s}}_{\mathbf{N}_{ctrl}} \tag{7.22} $$

Following the same procedure as previously, the magnetic moment of the control torque can be written as

$$ {}^{C}\mathbf{m} = \frac{-\lambda \mathbf{s}}{||{}^{C}\mathbf{B}||^2} \times {}^{C}\mathbf{B} \tag{7.23} $$

which gives a differentiated sliding variable looking like

$$\dot{\mathbf{s}} = \left[\frac{-\lambda \mathbf{I}^{-1}\mathbf{s}}{||^{C}\mathbf{B}||^2} \times {}^{C}\mathbf{B}\right] \times {}^{C}\mathbf{B} \tag{7.24}$$

once again assuming the equivalent torque to be zero.

The derivative of the Lyapunov Candidate Function $V = \mathbf{s}^{\intercal}\mathbf{I}\mathbf{s}$ becomes

$$\dot{V} = \frac{-\lambda}{||^{C}\mathbf{B}||^2}\big({}^{C}\mathbf{B} \times \mathbf{s}\big)\big({}^{C}\mathbf{B} \times \mathbf{s}\big) \tag{7.25}$$

The two last terms in eq. (7.25) retains the sign independent of the angle between ${}^{C}\mathbf{B}$ and $\mathbf{s}$. The conditions for the Lyapunov Candidate Function is therefore met and convergence towards the sliding manifold is secured.

Results of the developed SMC is shown in the next chapter.

Part IV

Results and Conclusion

8 Simulation Results

Simulation results of the Sliding Mode Controller from the previous chapter is in the following

The controller performance is judged on the time to settle and stay within an angular error of 10 degrees axis-wise, and at the same time use as little power (generated torque) as possible.

8.1 Sliding Mode Controller

The subsequent simulation of the Sliding Mode Controller has been conducted without any disturbances enabled, except state noise.

The sliding variable is given as

$$\mathbf{s} = \bar{\mathbf{\Omega}} + \mathbf{K}_s \bar{\mathbf{q}} \tag{8.1}$$

and the derivative of the sliding variable as

$$\dot{\mathbf{s}} = \mathbf{I}^{-1}\mathbf{N}_{ctrl} \tag{8.2}$$

where the control torque was decided by the sliding condition

$$\mathbf{N}_{ctrl} = -\lambda \mathbf{s} \tag{8.3}$$

The parameters $\mathbf{K}_s$ and λ has been chosen by an empiric approach to be

- $\mathbf{K}_s = 0.0005 \begin{bmatrix} 1 & 0 & 0 \\ 0 & 1 & 0 \\ 0 & 0 & 1 \end{bmatrix}$
- $\lambda = 0.00001$.

The specific parameters regarding the simulation are listed in Appendix A.

The simulation took 13.000 seconds, equivalent to just over two orbits, to converge. The combined mean power consumption at steady state was 0.6 mW. The largest deviation from the angular reference after settling was 1.8 degrees.

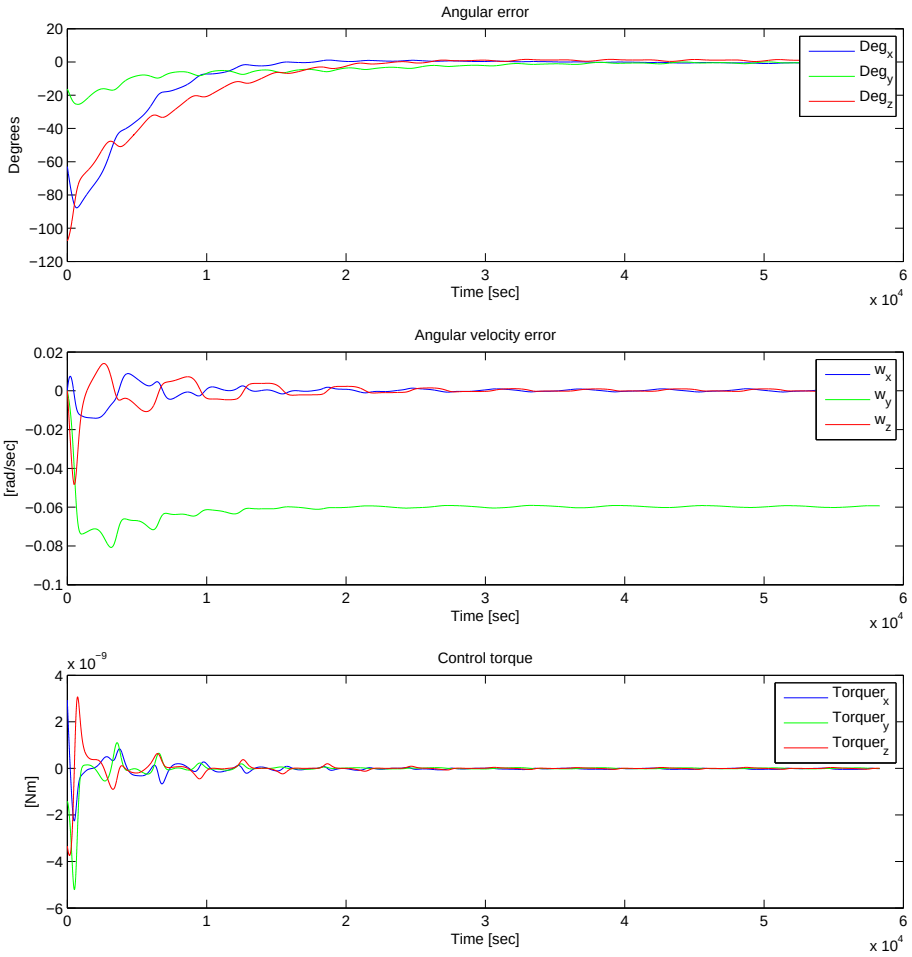

Figure 8.1: Simulation of Sliding Mode Controller.

8.2 Sliding Mode Controller with Perfect Disturbance Compensation

The subsequent simulation of the Sliding Mode Controller has been conducted with the equivalent torque enabled. The sliding variable is given as

$$\mathbf{s} = \bar{\mathbf{\Omega}} + \mathbf{K}_s \bar{\mathbf{q}} \tag{8.4}$$

and the derivative of the sliding variable as

$$\dot{\mathbf{s}} = \mathbf{I}^{-1}\mathbf{N}_{eq} + \mathbf{I}^{-1}\mathbf{N}_{ctrl} \tag{8.5}$$

where the control torque was decided by the sliding condition

$$\mathbf{N}_{ctrl} = -\lambda \mathbf{s} \tag{8.6}$$

and the equivalent torque is known from eq. (7.14)

$$\mathbf{N}_{eq} = \boldsymbol{\Omega} \times (\mathbf{I}\boldsymbol{\Omega}) + \omega_o \mathbf{I}(\mathbf{j}_o \times \boldsymbol{\Omega}) - \mathbf{I}\mathbf{K}_s \left[\boldsymbol{\Omega} q_4 - \boldsymbol{\Omega}\bar{\mathbf{q}}\right] - \mathbf{N}_{dist}. \tag{8.7}$$

The term $\mathbf{N}_{dist}$ inlcudes only the disturbance from the satellite magnetic dipole moment, as this is considered the largest cf. section 3.6. The values of the satellite dipole moment has been set to be $\mathbf{m}_{actual} = [0.002 \quad -0.002 \quad -0.006]^\intercal$ Am^2. The controller was implemented with perfect knowledge of the satellite dipole moment. This makes $\mathbf{N}_{dist}$ become

$$\mathbf{N}_{dist} = \mathbf{m}_{actual} \times {}^{C}\mathbf{B} \tag{8.8}$$

The parameters $\mathbf{K}_s$ and λ has been chosen empirically as described in the previous section, and has been kept the same

- $\mathbf{K}_s = 0.0005 \begin{bmatrix} 1 & 0 & 0 \\ 0 & 1 & 0 \\ 0 & 0 & 1 \end{bmatrix}$
- $\lambda = 0.00001$.

The specific parameters regarding the simulation are listed in Appendix A.

This simulation is similar to the first simulation regarding convergence time. It also settled in two orbits, however, the combined mean power consumption at steady state increased to was 5 mW in order to generate a counteracting magnetic dipole moment.

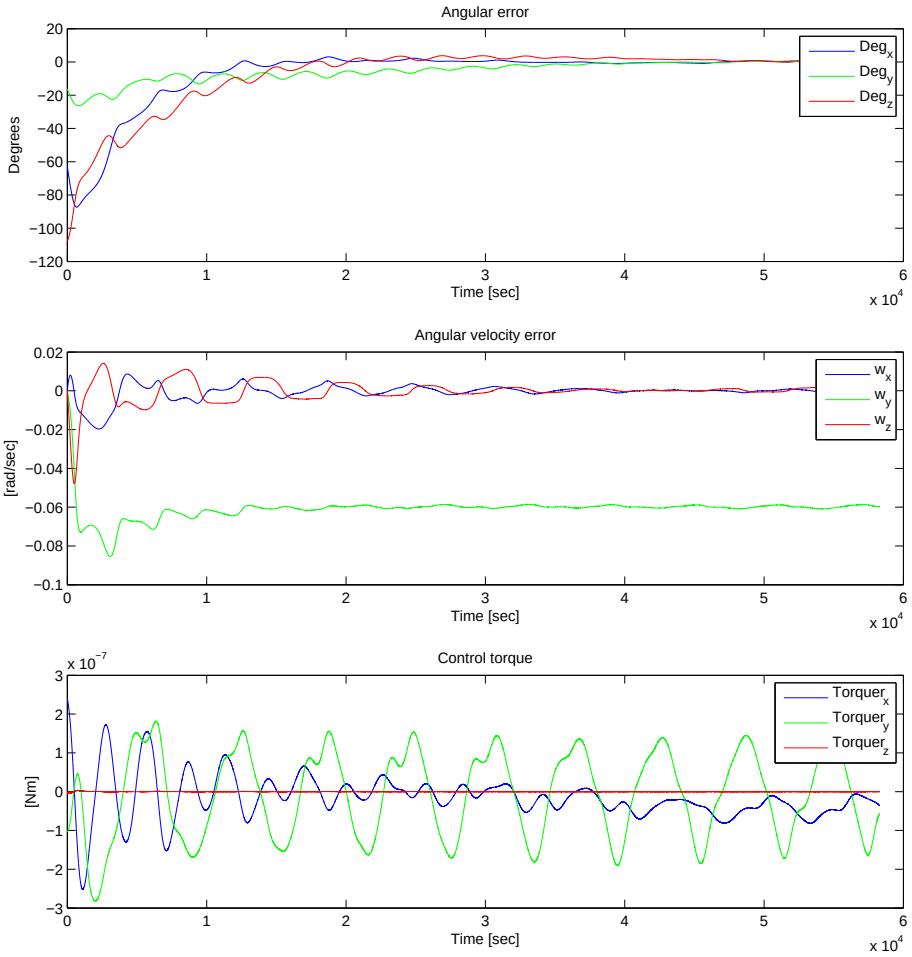

Figure 8.2: Simulation of Sliding Mode Controller with perfect disturbance compensation.

8.3 Sliding Mode Controller with Estimated Disturbance Compensation

The subsequent simulation of the Sliding Mode Controller has been conducted with the environmental disturbances enabled including the satellite dipole moment.

The Sliding Mode Controller has the same parameters as in the previous section, except for $\mathbf{N}_{dist}$. The enviromental disturbances from gravity gradient, solar radiation and aerodynamic pressure has been included, and the controller does no longer know the real dipole moment of the satellite. This was estimated

in chapter 6 to be $\mathbf{m}_{est} = [0.0021 \quad -0.0017 \quad -0.0056]^\intercal$ Am^2.

The simulation took 19.000 seconds to converge. The combined mean power consumption at steady state was 6 mW.

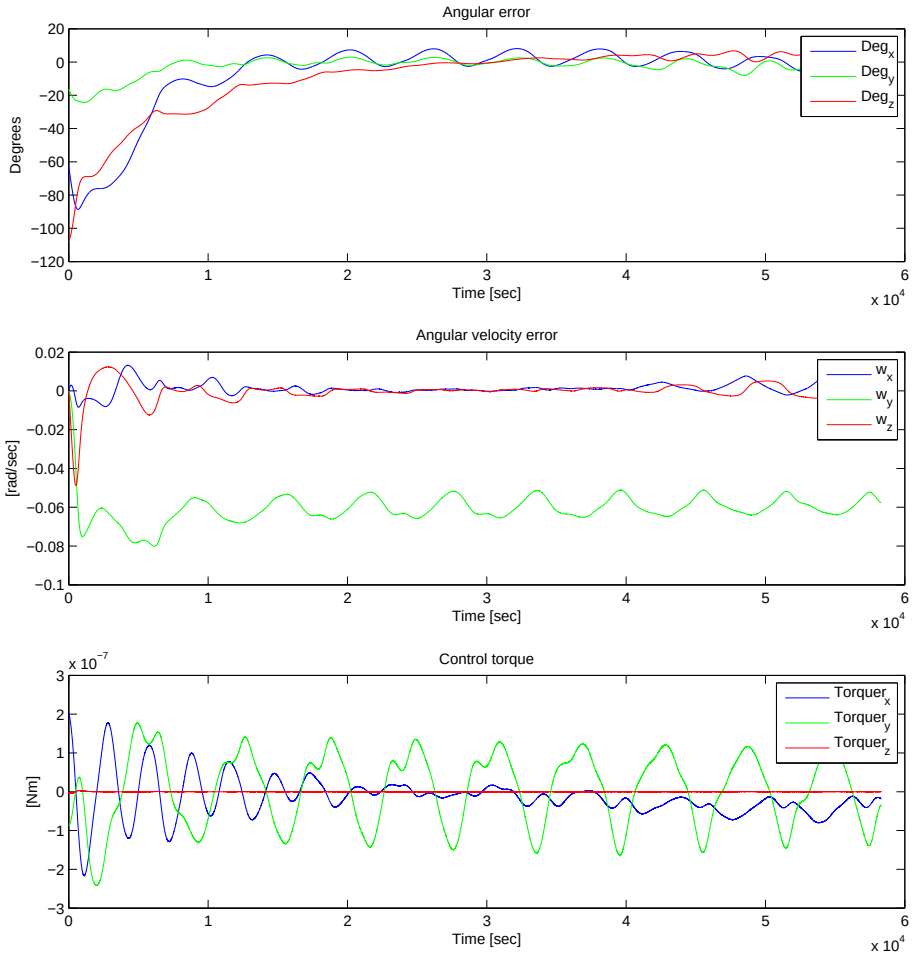

Figure 8.3: Simulation of Sliding Mode Controller with estimated disturbance compensation.

8.4 Sliding Mode Controller without Disturbance Compensation

The subsequent simulation of the Sliding Mode Controller has been conducted with all disturbances enabled, as in the previous section, but without the equivalent torque enabled.

The Sliding Mode Controller has the same parameters as in the previous section.

The simulation did not converge to the demand of 10 degree axis-wise error. Already at 11.000 seconds the error reaches 50 degrees and stays within this error throughout the simulation. The combined mean power consumption at steady state was 7.5 mW.

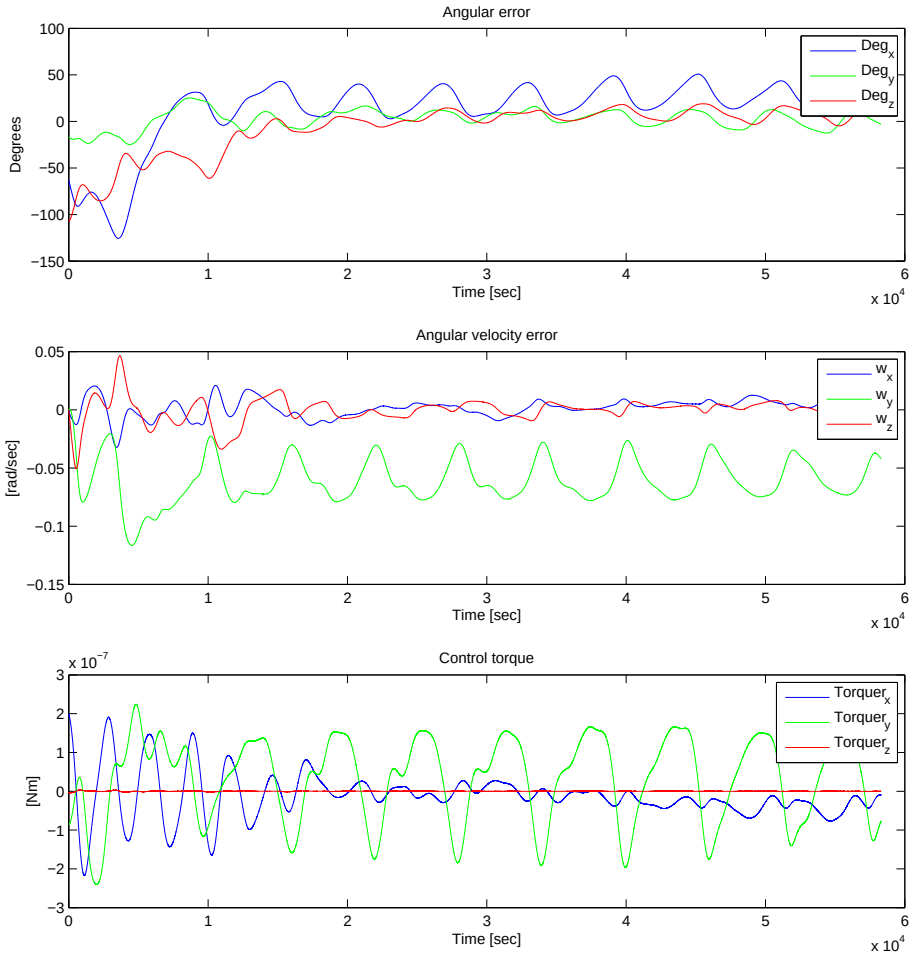

Figure 8.4: Simulation of Sliding Mode Controller without disturbance compensation.

9 Conclusion and Discussion

The developed Sliding Mode Controller performs as wanted. The simulation based on ideal criterions, where all disturbances where known and counteracted, had no trouble to converged to the nadir reference.

The magnetic dipole estimation resulted in a fair estimate. The estimate was performed on noisy states, where a real world implementation also would have the challenge of bias errors at the sensors, which is believed to make the dipole estimate worse.

When the estimated magnetic dipole moment is used in the sliding mode controller to counteract the torque caused by the satellite dipole moment, the performance of the controller is highly dependent on the accuracy of the estimate, as was seen from chapter 8.

If the results of the sliding mode controller is compared to that of the linear quadratic controller from B, it is clear that the sliding mode controller outperforms the linear quadratic controller.

The controller's dependency on the accuracy of the satellite dipole moment estimate can be a challenge when implementing a controller on an orbiting satellite, as even a small estimation error can cause an angular deviation from the reference attitude. Furthermore, the constant need to neutralize the dipole moment also has a downside when looking at power consumption. Any further work done to this project could be looking at a way to estimate the satellite dipole moment prior to launch, for instance as described in R. Moskowitz and R. Lynch [1964] where the estimation is based on measurements of the magnetic field around the satellite. If the dipole moment is known prior to launch it can be neutralized by inserting passive components, and thereby reduce the power consumption.

Part V

Appendix

Appendix content

- **A** Default Simulation Parameters
- **B** LQR Controller
- **C** Matlab Code

Simulation Parameters and Overview

A

The simulation parameters for the controllers are stated in the table below.

Satellite		
Mass	1	[kg]
Inertia	$diag$[0.0017464, 0.0022092, 0.0022388]	[−]
Max area	0.01732	$[m^2]$
Absorption constant	2	[−]
Dipole moment	[0.002 -0.002 -0.006]	$[Am^2]$
Drag coefficient	2	[−]
Centre of mass	[0.04907 0.04891 0.04297]	[m]
Coil area	0.049	$[m^2]$
Coil windings (pair)	550	[−]
Ephemeris		
Orbit height	600	[km]
Solar flux	$4.53 \cdot 10^{-6}$	$[kg/ms^2]$
Earth's magnetic moment	$7.96 \cdot 10^{15}$	[T]
Velocity	6000	[m/s]
Air density	$1.454 \cdot 10^{-13}$	$[kg/m^3]$

An overview of the simulation can be seen on figure A.1

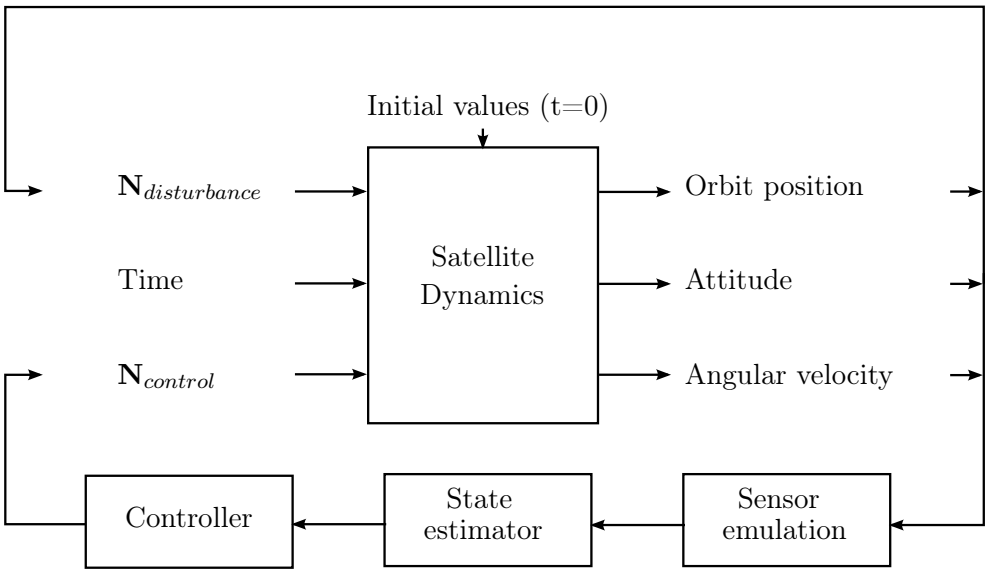

Figure A.1: Simplified simulation schematic

Linear Controller B

To compare the efficiency of the Sliding Mode Controller from chapter 7 a linear controller is made, based on the principle of a Linear Quadratic Regulator. This is intented to work as a Nadir pointing controller, tweaked to meet the following points

Maximum peak power consumption	15	mW
Maximum power consumption (1 orbit average)	10	mW
Maximum individual axis deviation	10	deg.
Maximum settle time	10	orbits

B.1 System model

The equations of motion from eq. (2.7) and eq. (2.16) are linearised to work in Nadir mode. The disturbances are neglected.

The kinematic equation remains the same:

$$\dot{\mathbf{q}} = \frac{1}{2}\mathbf{R}\left(\boldsymbol{\Omega}\right){}^{s}_{r}\mathbf{q}. \tag{B.1}$$

The external torques from eq. (2.16) gets replaced by the control torque from eq. (3.5)

$$\mathbf{I}_p\dot{\boldsymbol{\Omega}} = -\boldsymbol{\Omega} \times (\mathbf{I}_p\boldsymbol{\Omega}) + \mathbf{m}(t) \times \mathbf{B}(t). \tag{B.2}$$

B.2 Linearisation

The system model will have to be linearised about a desired operation point in order to be used in a linear controller. This is described in the following.

The attitude of the system is ment to perform in Nadir mode, which means that a fixed vector spanned in the Satellite body frame will always point towards the centre of Earth. In this report the spanned vector will be parallel to the z-axis of the Satellite frame.

When the z-axis of the satellite is pointing towards Earth and the x-axis is pointing in the orbit direction, the frames of the body and the orbit is aligning. This can be expressed as ${}^{S}_{O}\boldsymbol{\Omega} = \mathbf{0} = [0 \quad 0 \quad 0]^{\intercal}$ and ${}^{S}_{O}\mathbf{q} = [0 \quad 0 \quad 0 \quad 1]^{\intercal}$.

Kinematic

The linearization of the kinematic equation is made from the Inertial frame to the Satellite body frame, which behaves as a negative rotation around the y-axis: $[0 \quad -\omega_o \quad 0]$.

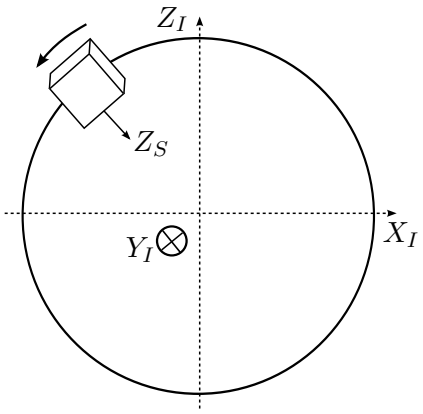

Figure B.1: Satellite orbiting the origin of the Inertial frame

With the kinematic equation from eq. (2.7) set up as

$$\begin{bmatrix} \dot{q}_1 \\ \dot{q}_2 \\ \dot{q}_3 \\ \dot{q}_4 \end{bmatrix} = \frac{1}{2}\mathbf{R}\left(\boldsymbol{\Omega}\right) \begin{bmatrix} q_1 \\ q_2 \\ q_3 \\ q_4 \end{bmatrix} \tag{B.3}$$

$$\begin{bmatrix} \dot{\bar{\mathbf{q}}} \\ \dot{q}_4 \end{bmatrix} = \frac{1}{2}\mathbf{R}\left(\boldsymbol{\Omega}\right) \begin{bmatrix} \bar{\mathbf{q}} \\ q_4 \end{bmatrix} \tag{B.4}$$

it can be rewritten as

$$\dot{\bar{q}} = \frac{1}{2}\left(q_4\boldsymbol{\Omega} - \boldsymbol{\Omega} \times \bar{\mathbf{q}}\right) \tag{B.5}$$

$$\dot{q}_4 = -\frac{1}{2}\boldsymbol{\Omega}^\intercal \bar{\mathbf{q}} \tag{B.6}$$

with $\bar{\mathbf{q}}$ being the imaginary part of the quaternion, $\begin{bmatrix} q_1 \\ q_2 \\ q_3 \end{bmatrix}$.

When linearized as a negative rotation around the Satellite body y-axis, the kinematic equation becomes

$$\dot{\bar{q}} = \frac{1}{2}\boldsymbol{\Omega} q_4 - \frac{1}{2}\boldsymbol{\Omega} \times \bar{\mathbf{q}} \approx \frac{1}{2}\boldsymbol{\Omega} \tag{B.7}$$

By replacing ${}^S_I\boldsymbol{\Omega}$ with the expression for ${}^S_O\boldsymbol{\Omega}_{CO}$ the following equation results in the linearized version of the kinematics

$$\delta\bar{\mathbf{q}} = \frac{1}{2}\delta\boldsymbol{\Omega} - \frac{1}{2}\begin{bmatrix} 0 & -\omega_o & 0 \end{bmatrix}^\intercal - \delta\bar{\mathbf{q}} \times \begin{bmatrix} 0 & -\omega_o & 0 \end{bmatrix}^\intercal \tag{B.8}$$

Dynamic

The dynamic equation is also linearized as a negative rotation around the Satellite body y-axis. The dynamic equation consists of the cross coupling and the generated control torque

$$\delta\dot{\mathbf{\Omega}} = \delta\left(-\mathbf{\Omega} \times \mathbf{I}_p\mathbf{\Omega}\right) + \mathbf{I}_p^{-1}\delta\mathbf{N}_{ctrl} \tag{B.9}$$

The cross coupling becomes

$$-\mathbf{\Omega} \times \mathbf{I}_p\mathbf{\Omega} = \begin{bmatrix}(I_y - I_z)\,\omega_y\omega_z\\(I_z - I_x)\,\omega_z\omega_x\\(I_x - I_y)\,\omega_x\omega_y\end{bmatrix} \tag{B.10}$$

When linearized around the y-axis eq. (B.10) becomes

$$-\mathbf{\Omega} \times \mathbf{I}_p\mathbf{\Omega} \approx \begin{bmatrix}\sigma_x\omega_o\delta\omega_z\\0\\\sigma_z\omega_o\delta\omega_x\end{bmatrix} \tag{B.11}$$

with

$$\sigma_x = \frac{I_y - I_z}{I_x} \qquad \sigma_y = \frac{I_z - I_x}{I_y} \qquad \sigma_z = \frac{I_x - I_y}{I_z} \tag{B.12}$$

B.3 State space model

Collecting the previously deduced linear models into a state space model yields the following result

$$\begin{bmatrix}\dot{\mathbf{\Omega}}\\\dot{\tilde{\mathbf{q}}}\end{bmatrix} = \begin{bmatrix}0 & 0 & \omega_0\sigma_x & 0 & 0 & 0\\0 & 0 & 0 & 0 & 0 & 0\\\omega_0\sigma_z & 0 & 0 & 0 & 0 & 0\\\frac{1}{2} & 0 & 0 & 0 & 0 & \omega_0\\0 & \frac{1}{2} & 0 & 0 & 0 & 0\\0 & 0 & \frac{1}{2} & \omega_0 & 0 & 0\end{bmatrix}\begin{bmatrix}\mathbf{\Omega}\\\tilde{\mathbf{q}}\end{bmatrix} \tag{B.13}$$

B.4 Controller structure

When the satellite is operating in Nadir mode it corresponds to letting the Satellite body frame align with the Orbit frame. Any deviation from this is an error, denoted with the subscript e and can be expressed as

$$\mathbf{\Omega}_e = {}^{S}_{O}\mathbf{\Omega} = {}^{S}\mathbf{\Omega} - {}^{O}\mathbf{\Omega} \tag{B.14}$$

for the angular velocities, and as

$$\mathbf{q}_e = {}^{O}_{S}\mathbf{q} = {}^{I}_{S}\mathbf{q} \otimes {}^{O}_{I}\mathbf{q} \tag{B.15}$$

for the quaternion error.

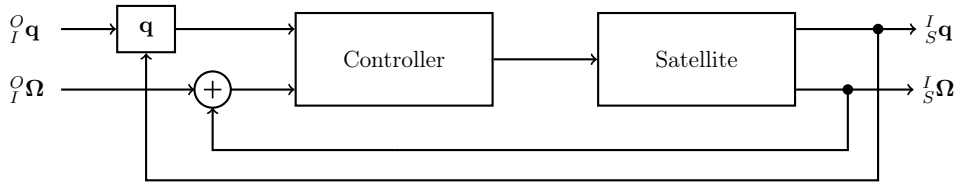

Figure B.2: Overview of the controller.

The system is linearized to work with an error of ${}^{S}_{O}\mathbf{q} = [0 \quad 0 \quad 0 \quad 1]$ and ${}^{S}_{O}\mathbf{\Omega} = [0 \quad 0 \quad 0]$. The model and reference is given in the Inertial frame while the state errors are fed into the controller after the quaternion operation and angular velocity substraction, respectively. This can be seen on figure B.2.

The controller is implemented as it would in a traditional MIMO system with the system equation given as

$$\dot{\mathbf{x}} = \mathbf{A}\mathbf{x} + \mathbf{B}\mathbf{u} \tag{B.16}$$

and full state observability and -feedback. The system states are estimated in a Kalman filter, performing calculations based on sensor reading and previous states. As the resulting state estimate from the Kalman filter is different from the true states, some precautions must be made. It is expected that the estimated states will act as an divergence around the true states. In the simulations, the estimator noise around the true states will be approximated as white noise with a mean of zero and a deviation of $\sigma^2 = 0.0001$ for the quaternion states and a deviation of $\sigma^2 = 0.000012$ for the angular velocity states [K. Vinther and K. Jensen [2010]].

B.5 LQR

A Linear Quadratic Regulator (LQR) is used as the linear controller, in order to compare it with a nonlinear controller. The LQR controller makes use of weighting matrices in order to calculate an optimal controller gain, which makes the system perform as desired.

A LQR can be designed and implemented to work in online- or offline mode, both having advantages and disadvantages compared to each other. The online LQR bases the controller gain on the present measurements, which should make it point more accurately. The drawback is the need for solving the

computationally heavy Riccati equation onboard the satellite. The offline controller applies a gain calculated prior to execution, based on the predicted satellite environment. This gives a lower pointing accuracy compared to the online controller but will be a lot easier to compute.

It has been decided to carry on with the offline controller, from now on refered to as a constant gain controller. The controller is inserted into the system equation from eq. (B.16), at the vector $\mathbf{u}$. This can be described as

$$\mathbf{u} = -\mathbf{L}\mathbf{x}_e \tag{B.17}$$

The controller uses the magnetorquers as actuators, which means that the feedback matrix, $\mathbf{L}$, only inputs to the dynamic equation from eq. (2.16) as an external force, as described in section 3.1. The $\mathbf{L}$ matrix therefore looks like

$$\mathbf{L} = \begin{bmatrix} L_{11} & L_{12} & L_{13} & L_{14} & L_{15} & L_{16} \\ L_{21} & L_{22} & L_{23} & L_{24} & L_{25} & L_{26} \\ L_{31} & L_{32} & L_{33} & L_{34} & L_{35} & L_{36} \end{bmatrix} \tag{B.18}$$

Performance function

The LQR optimizes a performance function to calculate the best possible controller gain for the system. The performance function uses penalties on the system states, input states and final states in order to deside how they perform compared to each other. The discrete time version of the performance function, with equal penalties for the final states, is given as

$$\mathcal{I} = \sum_{k=0}^{N} \mathbf{x}(k)^\intercal \mathbf{Q}_1 \mathbf{x}(k) + \mathbf{u}(k)^\intercal \mathbf{Q}_2 \mathbf{u}(k) \tag{B.19}$$

with

- $\mathbf{x}(k)$ being the system states at time k
- $\mathbf{u}(k)$ being the control signals at time k
- $\mathbf{Q}_1$ being the penalty weights for the system states
- $\mathbf{Q}_2$ being the penalty weights for the control signals

The resulting controller gain is calculated iteratively and requires knowledge about the orbit environment.

B-field approximation

The strength and direction of the magnetic flux field from Earth is depending on the distance from Earth and the type of orbit, and is varying with time. This can be seen on figure B.3 From the figure it is possible to see, that the

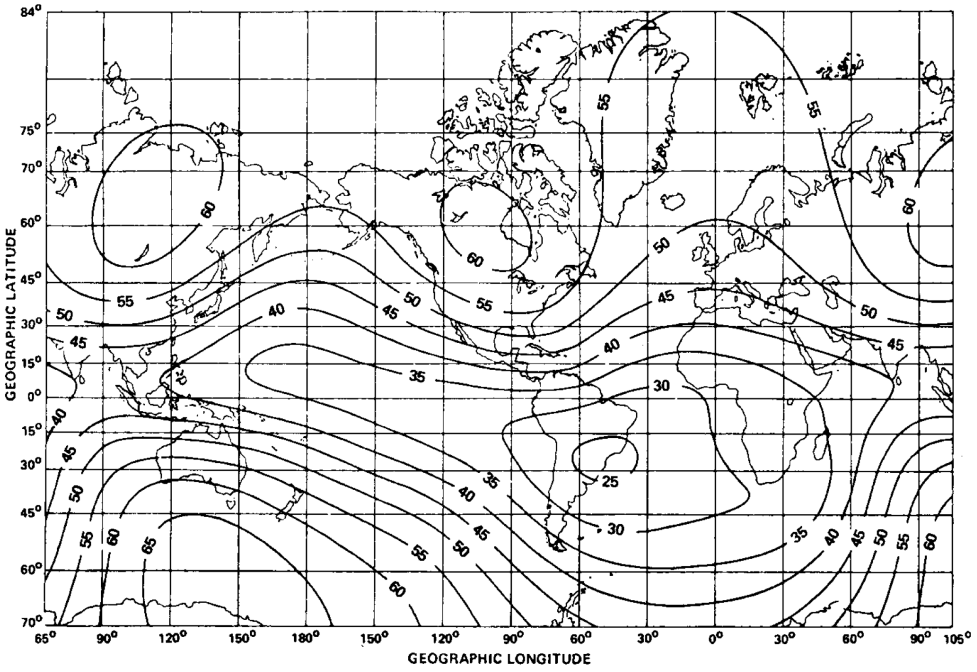

Figure B.3: Magnetic field intensity of Earth [Wertz [1994]].

change in intensity of the magnetic field is highly dependent on the orbit. An equatorial orbit would face less change in intensity, compared to a polar orbit.

In order to use the magnetorquers in an offline linear controller, an average of the magnetic field is nessesary. The average magnetic field can be calculated as

$$^{o}\hat{\mathbf{B}} = \frac{1}{T}\sum_{t=1}^{T} {}^{o}\mathbf{B}(t) \tag{B.20}$$

where ${}^{o}\mathbf{B}(t)$ is the magnetic flux vector from Earth given in the orbit frame for time t. The magnetic field has been captured from a simulation tool, set up with the predicted orbit parameters. The magnetic field at the simulation tool is based on the IGRF11 model. An example of a magnetic field experienced by the satellitte in polar orbit is shown in figure B.4

Weight penalty matrices

The weighting matrices, used in the performance function at eq. (B.19) to calculate the optimal controller gain, is shown here. The matrices have been set up with empirical guesses at first and iteratively adjusted in order to make

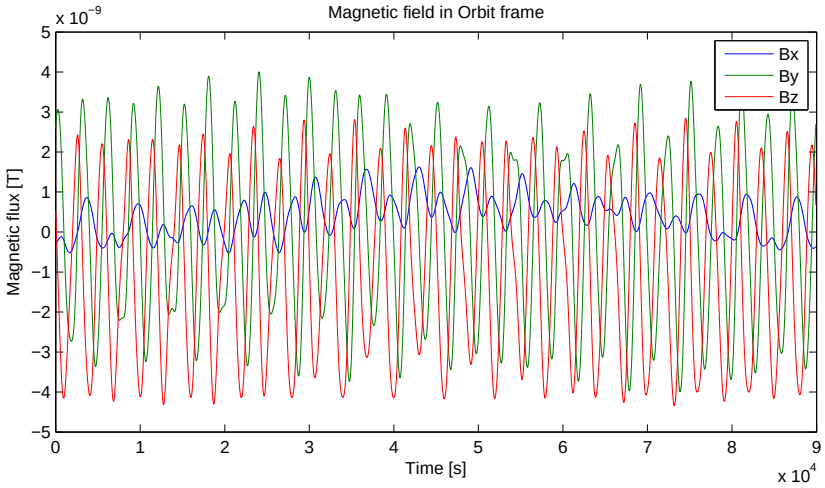

Figure B.4: Magnetic field captured in Orbit frame at polar orbit.

the system perform as described in the start of the chapter.

$$\mathbf{Q}_1 = \begin{bmatrix} 100 & 0 & 0 & 0 & 0 & 0 \\ 0 & 100 & 0 & 0 & 0 & 0 \\ 0 & 0 & 100 & 0 & 0 & 0 \\ 0 & 0 & 0 & 1 & 0 & 0 \\ 0 & 0 & 0 & 0 & 1 & 0 \\ 0 & 0 & 0 & 0 & 0 & 1 \end{bmatrix} \qquad \mathbf{Q}_2 = 10^{-4} \begin{bmatrix} 1 & 0 & 0 \\ 0 & 1 & 0 \\ 0 & 0 & 1 \end{bmatrix} \tag{B.21}$$

Simulation

The results from the simulation of the LQR are shown in the table below and in figure B.5. The simulation did not include any disturbances.

Power consumption:	
Settling phase (mean)	2,9 mW
Maintaining phase (mean)	0.724mW
Mean of 20 orbits	2mW
Maximum power consumption	12,2mW
Settling time	19.500 sec

The settling time is defined to be the time it takes the satellite from an arbitrary initial state till it settles with an axis-wise error below 10 degrees. The power consumption calculation is based on a simulation time of 20 orbits.

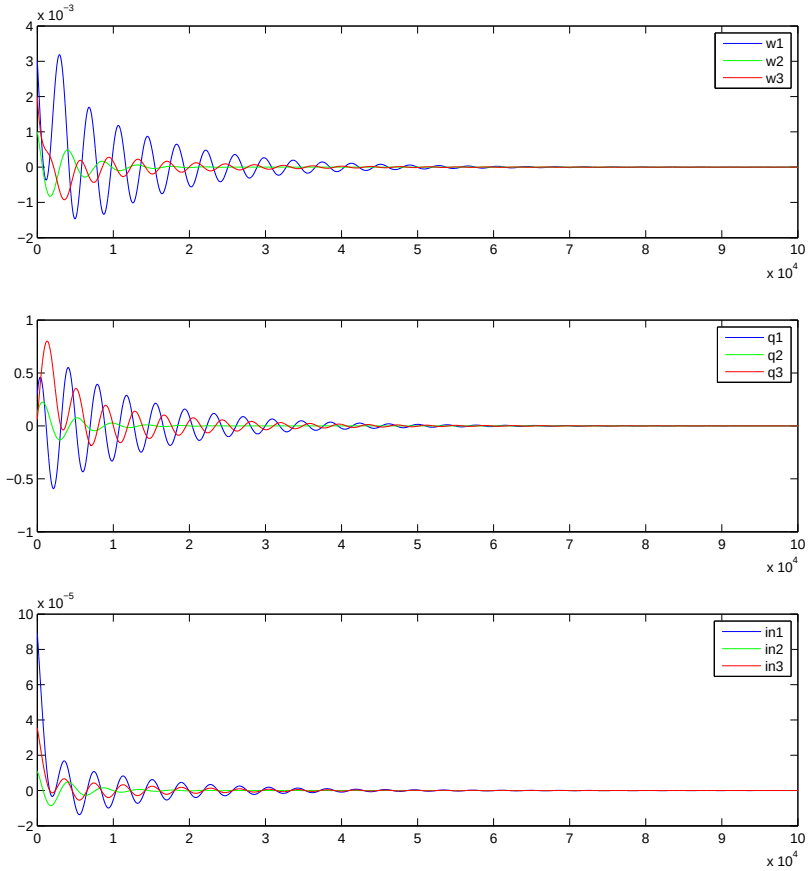

Figure B.5: Simulation of the system with chosen weights. Top: Angular velocity. Middle: Error angles. Bottom: Produced torque.

Matlab Code for Sliding Mode Controller

C

The following code is used as a function, with the following in- and outputs:

	Input vector u		
$\mathbf{u}_{1:3}$	Magnetic field measurement	$[Bx \quad By \quad Bz]$	[Tesla]
$\mathbf{u}_{4:7}$	Angular unit quaternion	$[q1 \quad q2 \quad q3 \quad q4]$	[–]
$\mathbf{u}_{8:10}$	Angular velocity	$[wx \quad wy \quad wz]$	[Rad/sec]

	Output vector		
$\mathbf{out}_{1:3}$	Control torque	$[Nctrl_x \quad Nctrl_y \quad Nctrl_z]$	[Nm]
$\mathbf{out}_{4:7}$	Equivalent torque	$[Neqv_x \quad Neqv_y \quad Neqv_z]$	[Nm]

MATLAB code:

```
function out = smc_function(u)
%#codegen

% ------------------------------------------------%
% -                  description                 -%
% ------------------------------------------------%
%Takes inputs from b-field, angle and ang. velocity.
%Creates control torque and dutycycle for driver

% ------------------------------------------------%
% -                  inputs                      -%
% ------------------------------------------------%
B_b = u(1:3);       %magnetic field [X Y Z] (Tesla)
quat = u(4:7);   %quaternion [q1 q2 q3 q(4/0)]
omega_ob = u(8:10);     %Angular velocity rate [Wx Wy Wz]


% ------------------------------------------------%
% -                  noise                       -%
% ------------------------------------------------%
% Comment in to add state noise
% noise = 0.001*randn(4,1);
% quat = quat+noise;
% quat = quat/norm(quat);
%
% noise = 0.00001*randn(3,1);
% omega_ob = omega_ob +noise;

% ------------------------------------------------%
% -                   Vars                       -%
% ------------------------------------------------%
% --- Environment ---
orbitTime = 5830;       % Orbit time in sec
omega_0 = (2*pi)/orbitTime; % Orbit rate

% --- Space ship ---
```

```
37 inertia = [0.0017464,0.0022092,0.0022388];
38 I = diag(inertia);
39
40 % --- Torquers ---
41 N = 550; % coil windings
42 A = [0 0 0]; %init
43 A(1) = 0.07*0.07; % coil area x
44 A(2) = 0.07*0.07; % y
45 A(3) = 0.07*0.07; % z
46 V = 5; % supply voltage
47 R_m = 950; % coil resistance
48 i_max = [V/R_m, V/R_m, V/R_m]'; % max current
49 m_max = [N*i_max(1)*A(1) , N*i_max(2)*A(2) , N*i_max(3)*A(3)]'; %
       max dipole
50
51 % --- Initial state vector ---
52 x0 = [quat ; omega_ob]; % [q1 q2 q3 q0 Wx Wy Wz]
53
54 w_ob_x = x0(5);  % Omega_x
55 w_ob_y = x0(6);  % Omega_y
56 w_ob_z = x0(7);  % Omega_z
57
58 omega_ob = [w_ob_x w_ob_y w_ob_z]'; %[Wx Wy Wz]
59 q = [x0(4) x0(1) x0(2) x0(3)]'; %[q0 q1 q2 q3] !!switch q4 to q1
       !!
60
61
62 q0 = q(1);
63 q_bar = [q(2) q(3) q(4)]';
64 % The rotation matrix FROM body TO orbit
65 S = [0 -q_bar(3) q_bar(2); q_bar(3) 0 -q_bar(1); -q_bar(2) q_bar
       (1) 0];
66 R_o_b = eye(3) + 2*q0*S + 2*(S);%^2;
67 % The rotation matrix FROM orbit TO body
68 R_b_o = R_o_b';
69
70
71 % Projection of the axes in the BODY frame
72 i_b = R_b_o(:,1);
73 j_b = R_b_o(:,2);
74 k_b = R_b_o(:,3); % <=> c_b_3 = [R13 R23 R33]'
75 % Gravitational torque
76 tau_b_g = 3*omega_0^2*(cross(k_b, (I*k_b)));
77
78
79
80 % ------------------------------------------%
81 % -              Controller                -%
82 % ------------------------------------------%
83 %References
84 q_r = [1 0 0 0]';
85 q4_r = q_r(1);
86 q_bar_r = [q_r(2) q_r(3) q_r(4)]';
```

```
87  Smatrix = [0 -q_bar_r(3) q_bar_r(2); q_bar_r(3) 0 -q_bar_r(1); -
        q_bar_r(2) q_bar_r(1) 0];
88  q_bar_tilde = (q4_r*q_bar) - (q0*q_bar_r) - (Smatrix*q_bar);
89  %q_tilde = [eta_tilde ; epsilon_tilde];
90
91  % Control gains
92  %Ks = 0.0005*diag([1 1 1]);
93  Ks = 0.0005*diag([1 1 1]);
94  %lambda_s = 0.00001;
95  lambda_s = 0.00001;
96
97  % Define sliding variable s and gain lambda_s
98  s = omega_b_ob + Ks*q_bar_tilde;
99
100 % Equivalent torques
101 %tau_eqv = cross(omega_b_ib, I*omega_b_ib) - tau_b_g + omega_0*I*
        cross(c_b_1, omega_b_ob)...
102 %    - 0.5*I*Ks*(omega_b_ib*eta + cross(omega_b_ib,epsilon));
103 mag_dipole_estimate = [0.0021 -0.0017 -0.0056]';
104 tau_eqv = -cross(B_b, mag_dipole_estimate);
105
106 %projected dipole
107 f = 1/(norm(B_b)^2);
108 tau_b_d = -lambda_s*s - tau_eqv; %desired torque
109 m_b = f*cross(B_b,tau_b_d);
110
111 % Magnetic torque.
112 tau_b_m = cross(m_b,B_b);
113
114 out = [tau_b_m' tau_eqv'];
```

Bibliography

B. Bandyopadhyay. *Discrete-time Sliding Mode Control.* Springer, first edition, 2006.

P. Hughes. *Spacecraft attitude dynamics.* Dover, first edition, 2004.

K. Vinther and K. Jensen. *Attitude Determination and Control System for AAUSAT3*, 2010.

H. Khalil. *Nonlinear Systems.* Prentice Hall, third edition, 2002.

M. Grewal and A. Andrews. *Kalman Filtering.* Wiley, third edition, 2008.

NASA. *Spacecraft Magnetic Torques*, 1969.

R. Moskowitz and R. Lynch. *Magnetostatic measurement of spacecraft magnetic dipole moment*, 1964.

R. Wisniewski. *Sattellite Attitude Control Using Only Electromagnetic Actuation*, 1996.

T. Inamori. *Magnetic dipole moment estimation and compensation for an accurate attitude control in nano-satellite missions*, 2010.

J. Wertz. *Spacecraft attitude determination and control.* Kluwer Academic, third edition, 1994.